

1      The effects of multi-dimensional drought on land cover change and  
2      vegetation productivity in continental Chile

3      Francisco Zambrano<sup>a,1,\*</sup>, Anton Vrieling<sup>b</sup>, Francisco Meza, Iongel Duran-Llacer, Francisco Fernández<sup>c</sup>,  
4      Alejandro Venegas-González, Nicolas Raab, Dylan Craven

<sup>a</sup> Universidad Mayor, Hémera Centro de Observación de la Tierra, Facultad de Ciencias, Escuela de Ingeniería en Medio Ambiente y Sustentabilidad, Santiago, Chile, 7500994

<sup>b</sup> University of Twente, Faculty of Geo-Information Science and Earth Observation (ITC), Enschede, The Netherlands,

<sup>c</sup> Universidad San Sebastián,

---

5      **Abstract**

The north-central region of Chile has been the focus of research studies due to the persistent decrease in water supply, which is impacting the hydrological system and vegetation development. This persistent period of water scarcity has been defined as a megadrought. The aim of our study is to evaluate the land cover change over continental Chile and to examine how this is connected to drought indices of water supply, atmospheric evaporative demand (AED), soil moisture, and their effects on vegetation productivity. The drought indices were derived using monthly ERA5-Land reanalysis data spanning from 1981 to 2023. The Moderate-Resolution Imaging Spectroradiometer (MODIS) datasets were utilized to obtain information on annual land cover and monthly vegetation productivity. We analyzed short- (1, 3, 6 months) to long-term (12, 24, 36 months) time scales of drought. Our results showed that land cover change was highest in the south-central part of the country, reaching changes as high as 36% in the surface type. The water demand has increased for the whole country, with a major increase in the north. The AED and soil moisture evidence a decreasing trend, which decreases at longer time scales and from north to south. The extreme south part of the country shows an increase in supply. Vegetation productivity has a negative trend in the north-central region for all land cover types. On the other hand, forests seem to be the most resistant type to drought. The types that show to be most affected by variation in climate conditions are shrublands, savannas, and croplands. The drought indices that have the capability of explaining to a major degree the variance in vegetation productivity are the ones that consider soil moisture for twelve months and the combined effect of precipitation and AED for 24 and 12 months. The results indicate that the north-central region is the most sensitive to water supply deficits lasting longer than a year.

6      **Keywords:** drought, land cover change, satellite

---

7      **1. Introduction**

8      Drought is often classified as meteorological when there is a decrease in precipitation below the mean  
9      average of several years (more than 30 years), hydrological when these anomalies last for long periods (months  
10     to years) and affect water systems, and agricultural when the deficit impacts plant health anomalies and  
11     leads to decreased productivity (Wilhite and Glantz, 1985). However, it is important to note that drought

---

\*Corresponding author

Email addresses: francisco.zambrano@umayor.cl (Francisco Zambrano), a.vrieling@utwente.nl (Anton Vrieling), francisco.fernandez@uss.cl (Francisco Fernández)

<sup>1</sup>This is the first author footnote.

is also influenced by human activities, which were not considered in the definitions. Thus, Van Loon et al. (2016) and AghaKouchak et al. (2021) have given an updated definition of drought for the Anthropocene, suggesting that it should be considered the feedback of humans' decisions and activities that drives the anthropogenic drought. Simultaneously, drought leads to heightened tree mortality and induces alterations in land cover and land use, ultimately affecting ecosystems (Crausbay et al., 2017). Even though many ecological studies have misinterpreted how to characterize drought, for example, sometimes considering "dry" conditions as "drought" (Slette et al., 2019). Then, Crausbay et al. (2017) proposed the ecological drought definition as "an episodic deficit in water availability that drives ecosystems beyond thresholds of vulnerability, impacts ecosystem services, and triggers feedback in natural and/or human systems." In light of current global warming, it is crucial to study the interaction between drought and ecosystems in order to understand their feedback and impact on water security. (Bakker, 2012)

Human-induced greenhouse gas emissions have increased the frequency and/or intensity of drought as a result of global warming, according to the sixth assessment report (AR6) of the Intergovernmental Panel on Climate Change (IPCC) (Calvin et al., 2023). The evidence supporting this claim has been strengthened since AR5 (IPCC, 2013). Recent studies, however, have produced contrasting findings, suggesting that drought has not exhibited a significant trend over the past forty years. (Vicente-Serrano et al., 2022; Kogan et al., 2020). Vicente-Serrano et al. (2022) analyzed the meteorological drought trend on a global scale, finding that only in a few regions has there been an increase in the severity of drought. Moreover, they attribute the increase in droughts over the past forty years solely to an increase in atmospheric evaporative demand (AED), which in turn enhances vegetation water demand, with important implications for agricultural and ecological droughts. Also, they state that "the increase in hydrological droughts has been primarily observed in regions with high water demand and land cover change". Similarly, Kogan et al. (2020) analyzed the drought trend using vegetation health methods, finding that for the globe, hemispheres, and main grain-producing countries, drought has not expanded or intensified for the last 38 years. Further, the Masson-Delmotte (2021) suggests that there is a high degree of confidence that rising temperatures will increase the extent, frequency, and severity of droughts. Also, AR6 (Calvin et al., 2023) predicts that many regions of the world will experience more severe agricultural and ecological droughts even if global warming stabilizes at 1.5°–2°C. To better evaluate the impact of drought trends on ecosystems, assessments are needed that relate meteorological and soil moisture variables to their effects on vegetation.

From 1960 to 2019, land use change has impacted around one-third of the Earth's surface, which is four times more than previously thought (Winkler et al., 2021). Multiple studies aim to analyze and forecast changes in land cover globally (Winkler et al., 2021; Song et al., 2018) and regionally (Chamling and Bera, 2020; Homer et al., 2020; Yang and Huang, 2021). Some others seek to analyze the impact of land cover change on climate conditions such as temperature and precipitation (Luyssaert et al., 2014; Pitman et al., 2012). There is less research on the interaction between drought and land cover change (Chen et al., 2022; Akinyemi, 2021; Peng et al., 2017). Peng et al. (2017) conducted a worldwide investigation utilizing net primary production to examine the spatial and temporal variations in vegetation productivity at global level. The study aimed to assess the influence of drought by comparing the twelve-month Standardized Precipitation Evapotranspiration Index (SPEI) and land cover change. According to their findings, drought is responsible for 37% of the decline in vegetation productivity, while water availability accounts for 55% of the variation. Chen et al. (2022) studied the trend of vegetation greenness and productivity and its relation to meteorological drought (SPEI of twelve months in December) and soil moisture at the global level. The results showed lower correlations (<0.2) for both variables. Akinyemi (2021) evaluates drought trends and land cover change using vegetation indices in Botswana in a semi-arid climate. These studies mostly looked at how changes in land cover and vegetation productivity are related to a single drought index (SPEI) over a single time period of 12 months. SPEI takes into account the combined effect of precipitation and AED as a water balance, but it does not allow us to know the contribution of each variable on its own. Some things worth investigating in terms of land cover change and vegetation productivity are: i) How do they respond to short- to long-term meteorological and soil moisture droughts? ii) How is the drought impacting land cover changes? And iii) How do they behave in humid and arid climatic zones regarding drought? Likewise, there is a lack of understanding of how the alteration in water supply and demand is affecting land cover

63 transformations.

64 For monitoring drought, the World Meteorological Organization recommends the SPI (Standardized Pre-  
65 cipitation Index) ([WMO et al., 2012](#)). The SPI is a multi-scalar drought index that only uses precipitation  
66 to assess short- to long-term droughts. The primary cause of drought is precipitation anomalies, and tem-  
67 perature usually makes it worse ([Luo et al., 2017](#)). Nowadays, there is an increase in attention toward  
68 using AED separately to monitor droughts ([Vicente-Serrano et al., 2020](#)). One reason is due to its attri-  
69 bution to increasing flash droughts in water-limited regions ([Noguera et al., 2022](#)). [Vicente-Serrano et al.](#)  
70 ([2010](#)) proposed the Standardized Precipitation Evapotranspiration Index (SPEI), which incorporated the  
71 temperature effect by subtracting AED from precipitation. SPEI allows for analysis of the combined effect  
72 of precipitation and AED. Since its formulation, it has been used worldwide for the study and monitoring  
73 of drought ([Gebrechorkos et al., 2023](#); [Liu et al., 2024](#)). [Hobbins et al. \(2016\)](#) and [McEvoy et al. \(2016\)](#)  
74 developed the Evaporative Demand Drought Index (EDDI) to monitor droughts solely using the AED, and  
75 it has proven effective in monitoring flash droughts ([Li et al., 2024](#); [Ford et al., 2023](#)). For soil moisture,  
76 several drought indices exist, such as the Soil Moisture Deficit Index (SDMI) ([Narasimhan and Srinivasan,](#)  
77 [2005](#)) and the Soil Moisture Agricultural Drought Index (SMADI) ([Souza et al., 2021](#)). [Hao and AghaK-](#)  
78 [ouchak \(2013\)](#) and [AghaKouchak \(2014\)](#) proposed the Standardized Soil Moisture Index (SSI), which has  
79 a similar formulation as the SPI, SPEI, and EDDI. Thus, there are plenty of drought indices that allow  
80 for a comprehensive assessment of drought from short- to long-term scales and consider variables from the  
81 earth's water balance on their own (e.g., precipitation, AED, soil moisture). Using this information, we can  
82 advance our understanding of the impact of drought on ecosystems.

83 Chile's diverse climatic and ecosystem types ([Beck et al., 2023](#); [Luebert and Pliscoff, 2022](#)) make it an  
84 ideal natural laboratory for studying climate and ecosystems. Additionally, the country has experienced  
85 severe drought conditions that have had significant effects on vegetation and water storage. North-central  
86 Chile has faced a persistent precipitation deficit since 2010, defined as a mega drought. ([Garreaud et al.,](#)  
87 [2017](#)), which has impacted the Chilean ecosystem. This megadrought was defined by the Standardized  
88 Precipitation Index (SPI) of twelve months in December having values below one standard deviation. Some  
89 studies have addressed how this drought affects single ecosystems in terms of forest development ([Miranda](#)  
90 [et al., 2020](#); [Venegas-González et al., 2018](#)), forest fire occurrence ([Urrutia-Jalabert et al., 2018](#)), and crop  
91 productivity ([Zambrano, 2023](#); [Zambrano et al., 2018, 2016](#)). We found one study regarding land cover and  
92 drought in Chile. The study by [Fuentes et al. \(2021\)](#) evaluates water scarcity and land cover change in Chile  
93 between 29° and 39° of south latitude. [Fuentes et al. \(2021\)](#) used the SPEI of one month for evaluating  
94 drought, which led to misleading results. For example, they did not find a temporal trend in the SPEI but  
95 found a decreasing trend in water availability and an increase trend on AED, which in turn should have  
96 been capable of being captured with longer time scales of the SPEI. The term "megadrought" in Chile is  
97 used to describe a prolonged water shortage that lasts for several years, resulting in a permanent deficit  
98 that impacts the hydrological system ([Boisier et al., 2018](#)). Therefore, it is crucial to evaluate temporal  
99 scales that consider the cumulative impact over a period of several years. There is limited understanding  
100 of the correlation between drought and the environment in Chile. Therefore, it is crucial to have a deeper  
101 understanding of how meteorological and soil moisture droughts impact the dynamics of the environment  
102 in order to make informed decisions on how to adapt.

103 Here, we analyze the multi-dimensional impacts of drought across ecosystems in continental Chile. More  
104 specifically, we aim to assess: i) short- to long-term temporal trends in multi-scalar drought indices; ii)  
105 temporal changes in land-use cover and the direction and magnitude of their relationships with trends in  
106 drought indices; and iii) the trend in vegetation productivity and its relationship with drought indices across  
107 Chilean ecosystems.

## 108 2. Study area

109 Continental Chile has diverse climate conditions with strong gradients from north to south and east to west  
110 ([Aceituno et al., 2021](#)) (Figure 1 a), which determines its great ecosystem diversity ([Luebert and Pliscoff,](#)

<sup>111</sup> 2022) (Figure 1 c). The Andes Mountains are a main factor in climate latitudinal variation (Garreaud, 2009).  
<sup>112</sup> “Norte Grande” and “Norte Chico” predominate in an arid desert climate with hot (Bwh) and cold (Bwk)  
<sup>113</sup> temperatures. At the south of “Norte Chico,” the climate changes to an arid steppe with cold temperatures  
<sup>114</sup> (Bsk). In these two northern regions, the land is mostly bare, with a small surface of vegetation types  
<sup>115</sup> such as shrubland and grassland. In the zones “Centro” and the north half of “Sur,” the main climate is  
<sup>116</sup> Mediterranean, with warm to hot summers (Csa and Csb). Land cover in “Centro” comprises a significant  
<sup>117</sup> amount of shrubland and savanna (50%), grassland (16%), forest (8%), and croplands (5%). An oceanic  
<sup>118</sup> climate (Cfb) predominates in the south of “Sur” and the north of “Austral.” Those zones are high in forest  
<sup>119</sup> and grassland. The southern part of the country has a tundra climate, and in “Austral,” it is a cold semi-arid  
<sup>120</sup> area with an extended surface of grassland, forest, and, to a lesser extent, savanna.

### <sup>121</sup> 3. Materials and Methods

#### <sup>122</sup> 3.1. Data

##### <sup>123</sup> 3.1.1. Gridded meteorological and vegetation data

<sup>124</sup> To analyze land cover change, we use the classification scheme by the IGBP (International Geosphere-  
<sup>125</sup> Biosphere Programme) from the product MCD12Q1 collection 6.1 from MODIS. The MCD12Q1 has a yearly  
<sup>126</sup> frequency from 2001 to 2022 and defines 17 classes. To derive a proxy for vegetation productivity, we used  
<sup>127</sup> the Normalized Difference Vegetation Index (NDVI) from the product MOD13A3 collection 6.1 from MODIS  
<sup>128</sup> (Didan, 2015). MOD13A3 provides vegetation indices at 1km of spatial resolution and monthly frequency.  
<sup>129</sup> The NASA EOSDIS Land Processes Distributed Active Archive Center (LP DAAC), USGS Earth Resources  
<sup>130</sup> Observation and Science (EROS) Center, Sioux Falls, South Dakota, provided the MOD13A3 and MCD12Q1  
<sup>131</sup> from the online Data Pool, accessible at <https://lpdaac.usgs.gov/tools/data-pool/>.

Table 1: Description of the satellite and reanalysis data used

Product	Sub-product	Variable	Spatial Resolution	Period	Units	Short Name
ERA5L		Precipitation	0.1°	1981-2023	mm	P
		Maximum temperature			°C	$T_{max}$
		Minimum temperature			°C	$T_{min}$
		Volumetric Soil Water Content at 1m			m3/m3	SM
ERA5L*		Atmospheric Evaporative Demand	0.1°	1981-2023	mm	AED
		Normalized Difference Vegetation Index			2000-2023	NDVI
MODIS	MOD13A3.061	land cover IGBP scheme	1 km	2001-2022		land cover

\*Calculated from maximum and minimum temperatures derived from ERA5L with Eq. 1.

<sup>132</sup> For soil moisture, water supply, and water demand variables, we used ERA5L (ECMWF Reanalysis version  
<sup>133</sup> 5 over land) (Muñoz-Sabater et al., 2021), a reanalysis dataset that provides the evolution of atmospheric and  
<sup>134</sup> land variables since 1950. It has a spatial resolution of 0.1° (9 km), hourly frequency, and global coverage.  
<sup>135</sup> We selected the variables for total precipitation, maximum and minimum temperature at 2 meters, and  
<sup>136</sup> volumetric soil water layers between 0 and 100cm of depth (layer 1 to layer 3). Table 1 shows a summary  
<sup>137</sup> of the data and its main characteristics.

#### <sup>138</sup> 3.2. Trend of short- to long-term drought

##### <sup>139</sup> 3.2.1. Atmospheric Evaporative Demand (AED)

<sup>140</sup> In order to compute the drought indices that use water demand, it is necessary to first calculate the  
<sup>141</sup> AED. To do this, we employed the Hargreaves method (Hargreaves, 1994; Hargreaves and Samani, 1985) by  
<sup>142</sup> applying the following equation:

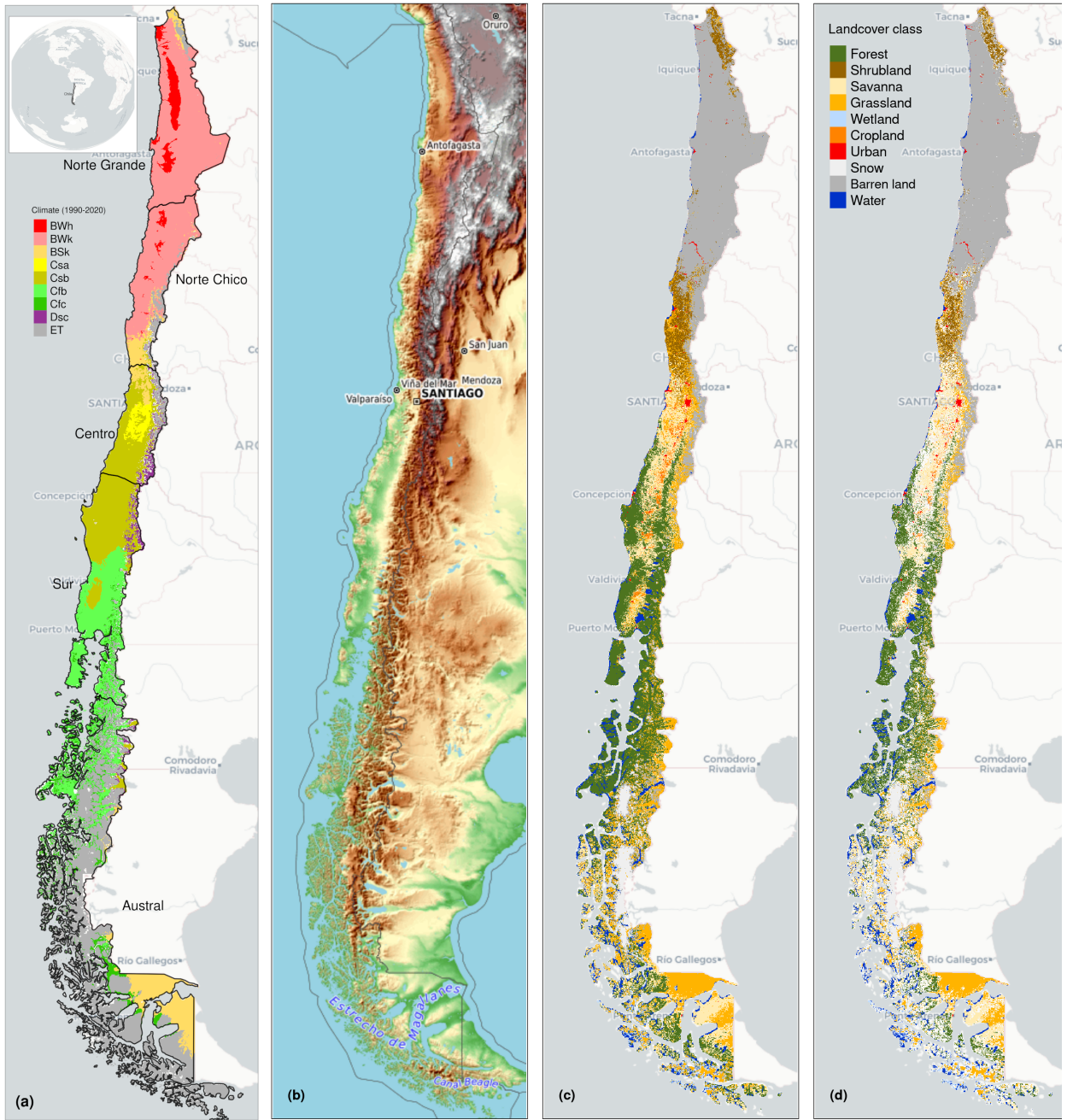


Figure 1: (a) Chile with the Koppen-Geiger climate classes and the five macrozones “Norte Grande”, “Norte Chico”, “Centro”, “Sur”, and “Austral”. (b) Topography reference map. (c) land cover classes for 2022. (d) Persistent land cover classes (> 80%) for 2001-2022

$$AED = 0.0023 \cdot Ra \cdot (T + 17.8) \cdot (T_{max} - T_{min})^{0.5} \quad (1)$$

where  $Ra$  ( $MJ\ m^2\ day^{-1}$ ) is extraterrestrial radiation;  $T$ ,  $T_{max}$ , and  $T_{min}$  are mean, maximum, and minimum temperature ( $^{\circ}C$ ) at 2m. For calculating  $Ra$  we used the coordinate of the latitud of the centroid of each pixel. We chose the method of Hargreaves to estimate AED because of its simplicity, which only

<sup>146</sup> requires temperatures and extrarrestrial radiation. Also, it has been recommended over other methods (e.g.,  
<sup>147</sup> Penman-Monteith) when the access to climatic variables is limited ([Vicente-Serrano et al., 2014](#)).

### <sup>148</sup> 3.2.2. Non-parametric calculation of drought indices

<sup>149</sup> To derive the drought indices of water supply and demand, soil moisture, and vegetation (i.e., the proxy  
<sup>150</sup> of productivity), we used the ERA5L dataset and the MODIS product, with a monthly frequency for 1981–  
<sup>151</sup> 2023 and 2000–2023, respectively. The drought indices correspond to a historical anomaly with regard to  
<sup>152</sup> a variable (e.g., meteorological, vegetation, or soil moisture). To account for the anomaly, the common  
<sup>153</sup> practice is to derive it following a statistical parametric methodology in which it is assumed that the  
<sup>154</sup> statistical distribution of the data is known ([Heim, 2002](#)). A wrong decision is usually the highest source of  
<sup>155</sup> uncertainty ([Laimighofer and Laaha, 2022](#)). In the case of Chile, due to its high degree of climatic variability,  
<sup>156</sup> it is complex to choose a proper distribution without previous research. Here, we follow a non-parametric  
<sup>157</sup> methodology for the calculation of the drought indices, in a similar manner as the framework proposed by  
<sup>158</sup> [Farahmand and AghaKouchak \(2015\)](#); [Hobbins et al. \(2016\)](#); [McEvoy et al. \(2016\)](#).

<sup>159</sup> For the purpose of monitoring water supply drought, we used the well-known Standardized Precipitation  
<sup>160</sup> Index (SPI), which relies on precipitation data. To evaluate water demand, we chose the Evaporative  
<sup>161</sup> Demand Drought Index (EDDI), developed by [Hobbins et al. \(2016\)](#) and [McEvoy et al. \(2016\)](#), which is based  
<sup>162</sup> on the AED. The United States currently monitors drought using the EDDI (<https://psl.noaa.gov/eddi/>)  
<sup>163</sup> as an experimental index. To consider the combined effect of water supply and demand, we selected the  
<sup>164</sup> SPEI ([Vicente-Serrano et al., 2010](#)). For SPEI, an auxiliary variable  $D = P - AED$  is calculated. Soil  
<sup>165</sup> moisture is the main driver of vegetation productivity, particularly in semi-arid regions ([Li et al., 2022](#)).  
<sup>166</sup> Hence, for soil water drought, we used the SSI (Standardized Soil Moisture Index) ([Hao and AghaKouchak,](#)  
<sup>167</sup> [2013](#); [AghaKouchak, 2014](#)). In our case, for the SSI, we used the average soil moisture from ERA5L at 1m  
<sup>168</sup> depth. Finally, for the proxy of productivity, we used the zcNDVI proposed by [Zambrano et al. \(2018\)](#),  
<sup>169</sup> which was derived from the monthly time series of NDVI retrieved from MOD13A1. All the indices are  
<sup>170</sup> multi-scalar and can be used for the analysis of short- to long-term droughts.

<sup>171</sup> To derive the drought indices, first we must calculate the sum of the variables with regard to the time scale  
<sup>172</sup> (s). In this case, for generalization purposes, we will use  $V$ , referring to variables  $P$ ,  $AED$ ,  $D$ ,  $NDVI$ , and  
<sup>173</sup>  $SM$  (Table 1). We cumulated each  $V$  over the time series of  $n$  values (months), and for the time scales  $s$ :

$$A_{si} = \sum_{i=n-s-i+2}^{n-i+1} V_i \quad \forall i \geq n-s+1 \quad (2)$$

<sup>174</sup> The  $A_{si}$  corresponds to a moving window (convolution) that sums the variable for time scales  $s$  from  
<sup>175</sup> the last month, month by month, until the first month in which it could sum for  $s$  months. An inverse  
<sup>176</sup> normal approximation ([Abramowitz and Stegun, 1968](#)) obtains the empirically derived probabilities once  
<sup>177</sup> the variable cumulates over time for the scale  $s$ . Then, we used the empirical Tukey plotting position ([Wilks,](#)  
<sup>178</sup> [2011](#)) over  $A_i$  to derive the  $P(a_i)$  probabilities across a period of interest:

$$P(A_i) = \frac{i - 0.33}{n + 0.33'} \quad (3)$$

<sup>179</sup> The drought indices  $SPI$ ,  $SPEI$ ,  $EDDI$ ,  $SSI$ , and  $zcNDVI$  are obtained following the inverse normal  
<sup>180</sup> approximation:

$$DI(A_i) = W - \frac{C_0 + C_1 \cdot W + c_2 \cdot W^2}{1 + d_1 \cdot W + d_2 \cdot W^2 + d_3 \cdot W^3} \quad (4)$$

<sup>181</sup>  $DI$  is referring to the drought index calculated for the variable  $V$  (i.e., SPI, SPEI, EDDI, SSI, and zcNDVI).  
<sup>182</sup> The values for the constats are:  $C_0 = 2.515517$ ,  $C_1 = 0.802853$ ,  $C_2 = 0.010328$ ,  $d_1 = 1.432788$ ,  $d_2 =$

183 0.189269, and  $d_3 = 0.001308$ . For  $P(A_i) \leq 0.5$ ,  $W = \sqrt{-2 \cdot \ln(P(A_i))}$ , and for  $P(A_i) > 0.5$ , replace  $P(A_i)$   
184 with  $1 - P(A_i)$  and reverse the sign of  $DI(A_i)$ .

185 The drought indices were calculated for time scales of 1, 3, 6, 12, 24, and 36 months at a monthly frequency  
186 for 1981–2023 in order to be used for short- to long-term evaluation of drought. In the case of the proxy of  
187 vegetation productivity (zcNDVI) it was calculated for a time scale of six months at monthly frequency for  
188 2000–2023. For zcNDVI, we test time scales of 1, 3, 6, and 12 months; we choose to use six months because  
189 that shows a more stable representation of vegetation productivity.

### 190 3.2.3. Trend of drought indices

191 To estimate if there are significant positive or negative trends for the drought indices, we used the non-  
192 parametric test of Mann-Kendall ([Kendall, 1975](#)). To determine the magnitude of the trend, we used Sen's  
193 slope ([Sen, 1968](#)). Some of the advantages of applying this methodology are that the Sen's slope is not  
194 affected by outliers as regular regression does, and it is a non-parametric method that is not influenced by  
195 the distribution of the data. We applied Mann-Kendall to see if the trend was significant and Sen's slope  
196 to estimate the magnitude of the trend. We did this to the six time scales from 1981 to 2023 (monthly  
197 frequency) and the indices SPI, EDDI, SPEI, and SSI. Thus, we have trends per index and time scale (24 in  
198 total). Then, we extracted the trend aggregated by macrozone and per land cover persistent macroclasses.

### 199 3.3. Interaction of land cover and drought

#### 200 3.3.1. Land cover change

201 To analyze the land cover change, we use the IGBP scheme from the MCD12Q1 collection 6.1 from MODIS.  
202 This product has been previously used for studies of drought and land cover in Chile ([Fuentes et al., 2021](#);  
203 [Zambrano et al., 2018](#)). From the 17 classes, we regrouped into ten macroclasses, as follows: classes 1-4 to  
204 forest, 5-7 to shrublands, 8-9 to savannas, 10 as grasslands, 11 as wetlands, 12 and 14 to croplands, 13 as  
205 urban, 15 as snow and ice, 16 as barren, and 17 to water bodies. Thus, we have a land cover raster time series  
206 with the ten macroclasses for 2001 and 2023. We validate the land cover macroclasses regarding a highly  
207 detailed (30 m of spatial resolution) land cover map made for Chile by [Zhao et al. \(2016\)](#) for 2013-2014.  
208 Our results showed a global accuracy of ~0.82 and a F1 score of ~0.66. Section S2 in the Supplementary  
209 Material shows the procedure for validation.

210 We calculated the surface occupied per land cover class into the five macrozones (“Norte Grande” to  
211 “Austral”) per year for 2001–2023. After that, we calculated the trend’s change in surface per land cover  
212 type and macroclass. We used Mann-Kendall for the significance of the trend ([Kendall, 1975](#)) and Sen's  
213 slope to calculate the magnitude ([Sen, 1968](#)).

214 Later in this study, we will examine the variation in vegetation productivity across various land cover  
215 types and how water demand and supply, and soil moisture affect it. In order to avoid variations due to a  
216 change in the land cover type from year-to-year that will wrongly impact NDVI, we developed a persistence  
217 mask for land cover for 2001–2022. Thereby, we reduce an important source of variation on a regional  
218 scale. Therefore, we generated a raster mask for IGBP MODIS per pixel using macroclasses that remained  
219 unchanged for at least 80% of the years (2001–2022). This enabled us to identify regions where the land  
220 cover macroclasses are persistent.

#### 221 3.3.2. Relationship between land cover and drought trends

222 We wanted to explore the relationship between the trend in land cover classes and the trend in the drought  
223 indices. For this purpose, in order to have more representative results, we conducted the analysis over sub-  
224 basins within continental Chile. We use 469 basins, which have a surface area between 0.0746 and 24,000  
225 ( $km^2$ ), and a median area of 1,249 ( $km^2$ ). For each basin, we calculate the relative trend per land cover  
226 type, considering the proportion of the type relative to the total surface of the basin. Then, we extracted  
227 per basin the average trend of the drought indices SPI, SPEI, EDDI, SSI, and all their time scales 1, 3, 6,  
228 12, 24, and 36. Also, we extracted the average trend in the proxy of vegetation productivity (zcNDVI). We  
229 wanted to analyze which drought indices and time scales have a major impact on changes in land cover type.

230 We have 25 predictors, including drought indices and vegetation productivity. We analyzed the 25 predictors per type of landcover, thus running six random forest models. Random forest uses multiple decision trees and allows for classification and regression. Some advantages are that it allows to find no linear relationship, reduces overfitting, and allows to derive the variable importance. We used random forests for regression and trained 1000 forests. To obtain more reliable results, we resampled by creating ten folds, running a random forest per fold, and calculating the r-squared (rsq), root mean square error (RMSE), and variable importance.

237 The variable importance helps for a better understanding of the relationships by finding which variable has  
238 a higher contribution to the model. We calculate the variable's importance by permuting out-of-bag (OOB)  
239 data per tree and computing the mean standard error in the OOB. After permuting each predictor variable,  
240 we repeat the process for the resting variable. We repeated this process ten times (per fold) to obtain the  
241 performance metrics (rsq, RMSE, and variable importance).

#### 242 *3.4. Drought impacts on vegetation productivity*

243 We analyzed the trend of vegetation productivity over the unchanged land cover macroclasses. To achieve  
244 this, we used the persistent mask of land cover macroclasses. This way, we tried to reduce the noise in the  
245 vegetation due to a change in land cover from year to year.

246 We examine the drought indices of water demand, water supply, and soil moisture and their correlation  
247 with vegetation productivity. The objective is to determine the impact of soil moisture and water demand  
248 and supply on vegetation productivity. We want to address three main questions: Which of the drought  
249 variables—supply, demand, or soil moisture—most helps to explain the changes in plant productivity? Which  
250 of the short-term or long-term time scales of the drought variable has a bigger effect on vegetation productivity  
251 in Chile? And finally, how strong is the relationship between the variables and the drought index? Thus,  
252 we will be able to advance in understanding how climate is affecting vegetation, considering the impact on  
253 the five land cover types: forest, cropland, grassland, savanna, and shrubland.

254 We conducted an analysis on the linear correlation between the indices SPI, SPEI, EDDI, and SSI over time  
255 periods of 1, 3, 6, 12, 24, and 36 months with zcNDVI. We used a method similar to that used by [Meroni et al. \(2017\)](#) which compared the SPI with the cumulative FAPAR (Fraction of Absorbed Photosynthetically  
256 Active Radiation). A pixel-to-pixel linear correlation analysis was performed for each index within the  
257 persistent mask of land cover macroclasses. To begin, the Pearson coefficient of correlation is computed for  
258 each of the six time scales. A time scale is identified as the one that attains the highest correlation ( $p < 0.05$ ). Subsequently, the Pearson correlation coefficient corresponding to the time scales at which the value  
259 peaked was extracted. As a result, for each index, we generated two raster maps: 1) containing the raster  
260 with values of the time scales and drought index that reached the maximum correlation, and 2) having the  
261 magnitude of the correlation obtained by the drought index at the time scales.

#### 264 *3.5. Software*

265 For the downloading, processing, and analysis of the spatio-temporal data, we used the open source software  
266 for statistical computing and graphics, R ([R Core Team, 2023](#)). For downloading ERA5L, we used the  
267 `{ecmwfr}` package ([Hufkens et al., 2019](#)). For processing raster data, we used `{terra}` ([Hijmans, 2023](#)) and  
268 `{stars}` ([Pebesma and Bivand, 2023](#)). For managing vectorial data, we used `{sf}` ([Pebesma, 2018](#)). For  
269 the calculation of AED, we used `{SPEI}` ([Beguería and Vicente-Serrano, 2023](#)). For mapping, we use `{tmap}`  
270 ([Tennekes, 2018](#)). For data analysis, the suite `{tidyverse}` ([Wickham et al., 2019](#)) was used. For the random  
271 forest modeling, we used the `{tidymodels}` ([Kuhn and Wickham, 2020](#)) and `{ranger}` ([Wright and Ziegler,  
272 2017](#)) packages.

## 273 **4. Results**

### 274 *4.1. Trend of short- to long-term drought*

275 Figure 2 shows the spatial variation of the trend for the drought indices from short- to long-term scales.  
276 SPI and SPEI have a decreasing trend from “Norte Chico” to “Sur.” However, there is an increasing trend

<sup>277</sup> in “Austral.” The degree of the trend is stronger at higher time scales. The SSI indicates that in “Norte  
<sup>278</sup> Grande,” there are surfaces that have increased in the southwest part and in the northeast have decreased,  
<sup>279</sup> and is shown for all time scales. Similar to SPI and SPEI, SSI decreases at higher time scales. EDDI showed  
<sup>280</sup> a positive trend for the whole of continental Chile, with a higher trend toward the north and a descending  
<sup>281</sup> gradient toward the south. The degree of trend increases at higher time scales.

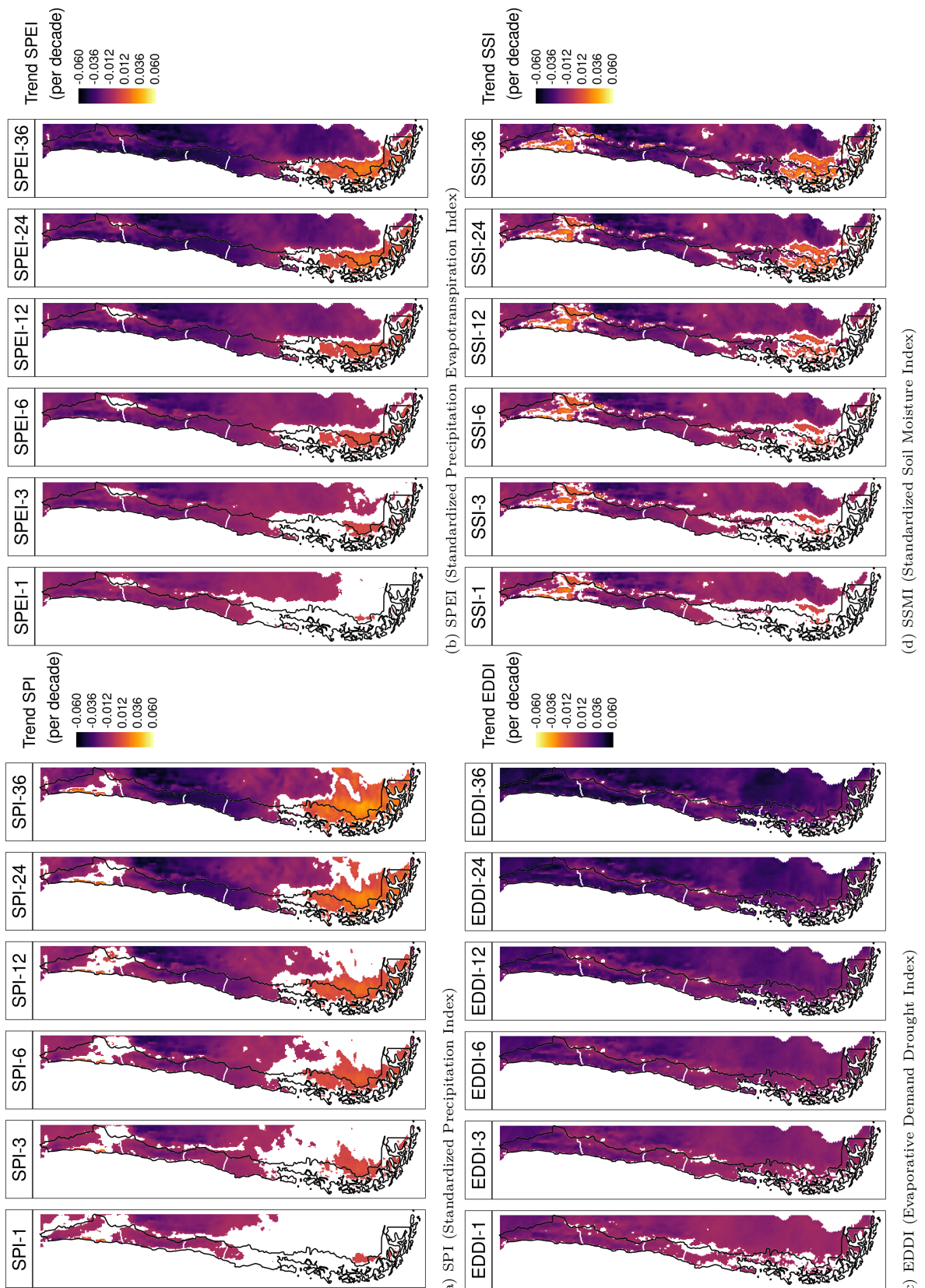


Figure 2: Linear trend of the drought index (\*) at time scales of 1, 3, 6, 12, 24, and 36 months for 1981-2023

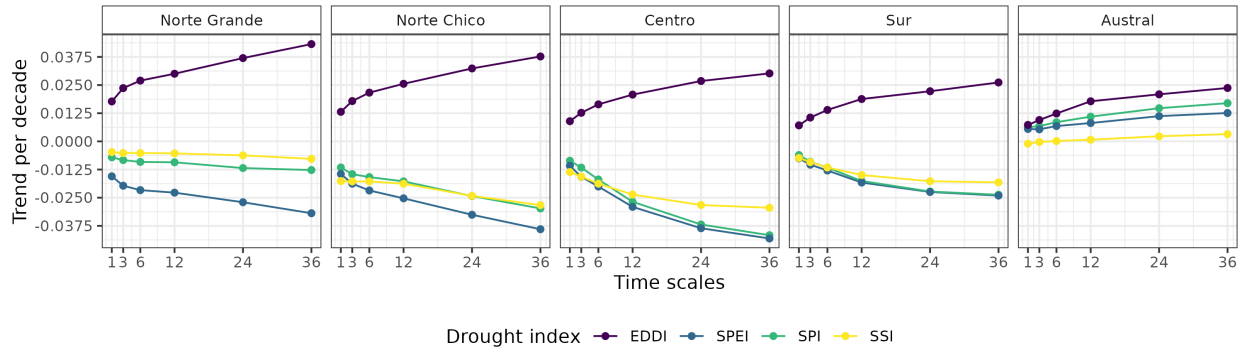


Figure 3: Trend per decade for the drought indices SPI, EDDI, SPEI, and SSI aggregated by macrozone.

In Figure 3, the averaged aggregation per macrozone, drought index, and time scale are shown. The macrozones that have the lowest trend are “Norte Chico” and “Centro,” where the SPI, SPEI, and SSI show that it decreases at longer time scales. Potentially explained due to the prolonged reduction in precipitation that has affected the hydrological system in Chile. At 36 months, it reaches trends between -0.03 and -0.04 (z-score) per decade for SPI, SPEI, and SSI. For “Sur,” the behavior is similar, decreasing at longer scales and having between -0.016 and -0.025 per decade for SPI, SPEI, and SSI. “Norte Grande” has the highest trend at 36 months for EDDI (0.042 per decade), and “Centro” has the lowest for SPI and SPEI. In “Norte Grande” and “Norte Chico,” which are in a semi-arid climate, it is evident that the EDDI has an effect on the difference between the SPI and SPEI index, which is not seen in the other macrozones. Contrary to the other macrozones, “Austral” showed an increase in all indices, being the highest for EDDI at 36 months (0.025) and the lowest for SSI, which shows only a minor increase in the trend.

#### 4.1.1. Interaction of land cover and drought

#### 4.2. Land cover change

Table 2: Surface of the land cover class that persist during 2001-2022

Surface [km <sup>2</sup> ]						
macrozone	Forest	Cropland	Grassland	Savanna	Shrubland	Barren land
Norte Grande		886		7,910		171,720
Norte Chico		90	4,283	589	16,321	84,274
Centro	3,739	1,904	7,584	19,705	844	12,484
Sur	72,995	1,151	7,198	15,906		2,175
Austral	60,351		54,297	19,007	249	7,218
Total	—	137,085	3,145	74,247	55,206	25,324
						277,870

For vegetation, we obtained and use hereafter five macroclasses of land cover from IGBP MODIS: forest, shrubland, savanna, grassland, and croplands. Figure 1c shows the spatial distribution of the macroclasses through Chile for the year 2022. Figure 1d shows the macroclasses of land cover persistance (80%) during 2021–2022, respectively (Table 2). Within continental Chile, barren land is the land cover class with the highest surface area ( $277,870 \text{ km}^2$ ). The largest type of vegetation, with  $137,085 \text{ km}^2$ , is forest. Grassland has  $74,247 \text{ km}^2$ , savanna  $55,206 \text{ km}^2$ , shrubland  $25,324 \text{ km}^2$ , and cropland  $3,145 \text{ km}^2$  (Table 2). The macrozones with major changes for 2001–2022 were “Centro,” “Sur,” and “Austral,” with 36%, 31%, and 34% of their surface changing the type of land cover, respectively (Figure 1 and Table 3). Figure 4 shows the summary of the proportion of surface per land cover class and macrozone, derived from the persistance mask over continental Chile.

From the trend analysis in Table 3, we can indicate that the “Norte Chico” shows an increase in barren land of  $111 \text{ km}^2 \text{ yr}^{-1}$  and a reduction in the class savanna of  $70 \text{ km}^2 \text{ yr}^{-1}$ . In the “Centro” and “Sur,” there

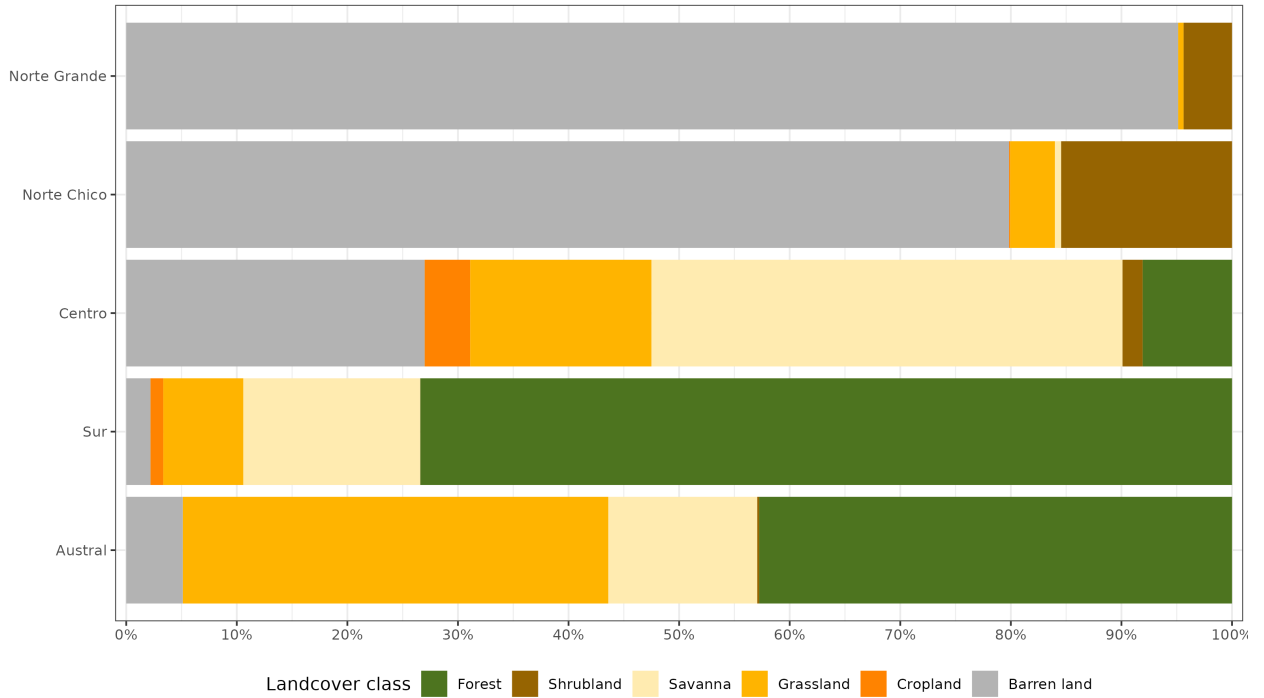


Figure 4: Proportion of land cover class from the persistent land cover for 2001-2022 ( $>80\%$ ) per macrozone

Table 3: The value of Sen's slope trend next to the time-series plot of surface per land cover class (IGBP MCD12Q1.016) for 2001–2022 through Central Chile. Values of zero indicate that there was not a significant trend. Red dots on the plots indicate the maximum and minimum values of surface.

macrozone	Trend of change [ $\text{km}^2 \text{ year}^{-1}$ ]											
	Forest		Cropland		Grassland		Savanna		Shrubland		Barren land	
	x	y	x	y	x	y	x	y	x	y	x	y
Norte Grande	0.0	0.0	0.0	0.0	0.0	0.0	0.0	0.0	0.0	0.0	0.0	0.0
Norte Chico	0.0	0.0	-12.1	0.0	0.0	0.0	-70.0	0.0	0.0	0.0	0.0	111.2
Centro	0.0	0.0	-22.4	83.2	0.0	-136.2	0.0	146.0	0.0	0.0	0.0	22.9
Sur	396.6	37.8	0.0	0.0	0.0	-318.8	0.0	0.0	172.1	-36.9	0.0	0.0
Austral	0.0	0.0	0.0	0.0	0.0	0.0	0.0	0.0	0.0	0.0	0.0	-93.2

are changes with an important reduction in savanna ( $136$  to  $318 \text{ km}^2 \text{ yr}^{-1}$ ), and an increase in shrubland and grassland. Showing a change for more dense vegetation types. The area under cultivation (croplands) appears to be shifting from the “Centro” to the “Sur.” Also, there is a high increase in forest ( $397 \text{ km}^2 \text{ yr}^{-1}$ ) in the “Sur,” replacing the savanna lost (Table 3).

#### 4.2.1. Relationship between drought indices and land cover change

According to Table 4, the random forest models for estimating the landcover trend from the trends in drought indices reach an r-squared between 0.32 and 0.39 for the types of forest, grassland, savanna, shrubland, and barren land. It is more likely that short- and medium-term increases in AED (EDDI-6 and EDDI-12) and short-term precipitation deficits (SPI-6 and SPEI-6) contributed to changes in grassland and bare land. The short-term increase of AED (EDDI-3 and EDDI-6) and the longer duration of the precipitation deficit (SPI-24, SPI-36, and SPEI-36) most likely contribute to the changes in shrubland. The changes

318 in savanna are associated with a short- and long-term increase in AED and a three-year precipitation deficit  
 319 (SPI-36). The increase in cumulative AED from 12 to 36 months is the strongest associated variable that  
 320 contributes to changes in forests, followed by the reduction of soil moisture over six and 36 months. The  
 321 supplementary material in Section S3 provides further details about the variable's importance.

Table 4: The five most important trends of drought indices in estimating the landcover trend per land cover type and the r-squared (rsq) reached by each random forest model.

Position	Forest (rsq=0.32)	Cropland (rsq=0.06)	Grassland (rsq=0.39)	Savanna (rsq=0.23)	Shrubland (rsq=0.23)	Barren_Land (rsq=0.32)
1	EDDI-36	EDDI-36	EDDI-6	EDDI-6	EDDI-6	EDDI-12
2	EDDI-24	SSI-36	EDDI-12	EDDI-12	SPI-36	EDDI-6
3	EDDI-12	EDDI-24	EDDI-24	SPI-36	SPEI-36	SPI-6
4	SSI-36	EDDI-12	SPEI-6	EDDI-36	EDDI-3	SPEI-6
5	SSI-6	SSI-24	SPI-6	EDDI-24	SPI-24	EDDI-24

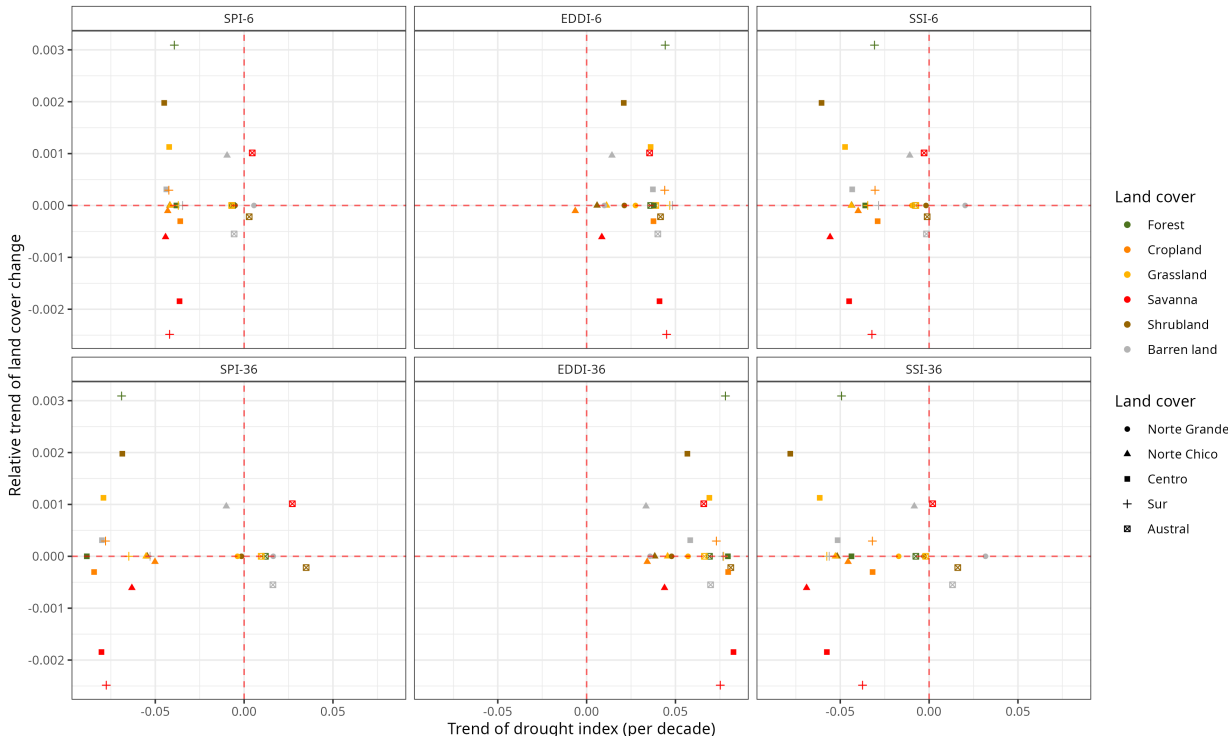


Figure 5: Relationship between the trend in land cover change (y-axis) and the trend in drought indices (x-axis) for the five macrozones. Vertical panels correspond to 1, 3, 6, 12, 24, and 36 months of the time scale by drought index. Horizontal panels show each drought index

322 We study the connection between the SPI, EDDI, and SSI drought indices and changes in land cover in  
 323 Figure 5. To do this, we compare the relative changes in land cover (in terms of the total surface area per  
 324 land cover type and macrozone) over six and thirty-six months. Figure 5 shows that the forest in the “Sur,”  
 325 shrubland and grassland in “Centro,” barren land in “Norte Chico,” and savanna in “Austral” showed an  
 326 increase in the surface of landcover associated with an increase in EDDI. Savanna in “Centro,” “Sur,” and

327 “Norte Chico” decreases with the increase in EDDI. The SPI and SSI showed similar behavior regarding  
 328 the trend in land cover type. A decrease in SPI and SSI is associated with an increase in the surface in  
 329 shrubland and grassland in “Centro,” forest in “Sur,” and barren land in “Norte Chico,” as well as a  
 330 decrease trend in savanna in “Norte Chico,” “Centro,” and “Sur.”

331 *4.3. Drought impacts on vegetation productivity within land cover*

332 *4.3.1. Trends in vegetation productivity*

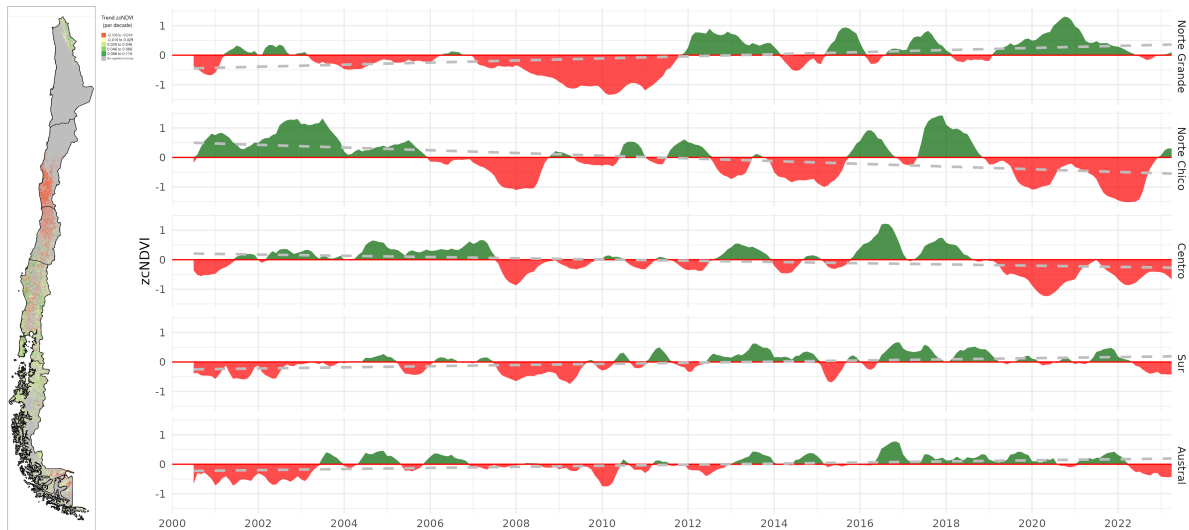


Figure 6: (a) Map of the linear trend of the index zcNDVI for 2000–2023. Greener colors indicate a positive trend; redder colors correspond to a negative trend and a decrease in vegetation productivity. Grey colors indicate either no vegetation or a change in land cover type for 2001–2022. (b) Temporal variation of zcNDVI-6 aggregated at macrozone level within continental Chile. Each horizontal panel corresponds to a macrozone from ‘Norte Grande’ to ‘Austral’.

333 In Figure 6 it is showed the spatial map of trends in zcNDVI (Figure 6a). In “Norte Grande,” vegetation  
 334 productivity, as per the z-index, exhibits a yearly increase of 0.027 for grassland and 0.032 for shrubland. In  
 335 the “Norte Chico,” savanna has the lowest trend of -0.062, cropland -0.047, shrubland -0.042, and grassland  
 336 -0.037. In “Centro,” shrubland reaches -0.07, savanna -0.031, cropland -0.024, forest -0.017, and grassland  
 337 -0.005 per decade. This decrease in productivity could be associated either with a reduction in vegetation  
 338 surface, a decrease in biomass, or browning ([Miranda et al., 2023](#)).

339 The temporal variation within the macrozones is showed in Figure 6b). There is a negative trend in “Norte  
 340 Chico” with -0.035 and “Centro” with -0.02 per decade. Vegetation reached its lowest values since the year  
 341 2019, with an extreme condition in early 2020 and 2022 in the “Norte Chico” and “Centro”. The “Sur”  
 342 and “Austral” show a positive trend of around 0.012 and 0.016, respectively per decade (Figure 6). Despite  
 343 the croplands suffering from drought just as badly as the native vegetation in “Norte Chico,” the savanna  
 344 and shrubland appears to be the region most affected by a negative trend in vegetation productivity across  
 345 Chile.

346 *4.3.2. Correlation between vegetation productivity and drought indices*

347 Figure 7 is a map that shows the highest coefficient of determination ( $r^2$ , or rsq) found in the  
 348 regression analysis between different drought indicators and plant productivity over time. The spatial  
 349 variation of time scales reached per index is mostly for time scales above 12 months. In the case of SSI,  
 350 the predominant scales are 6 and 12 months. For all indices, to the north, the time scales are higher and  
 351 diminish toward the south until the south part of “Austral” increases. In Figure 8, the map of Pearson  
 352 correlation values is shown. The EDDI reached correlations above 0.5 between “Norte Chico” and “Sur.”  
 353 The correlation changes from negative to positive toward the Andes Mountains and to the sea, just as in

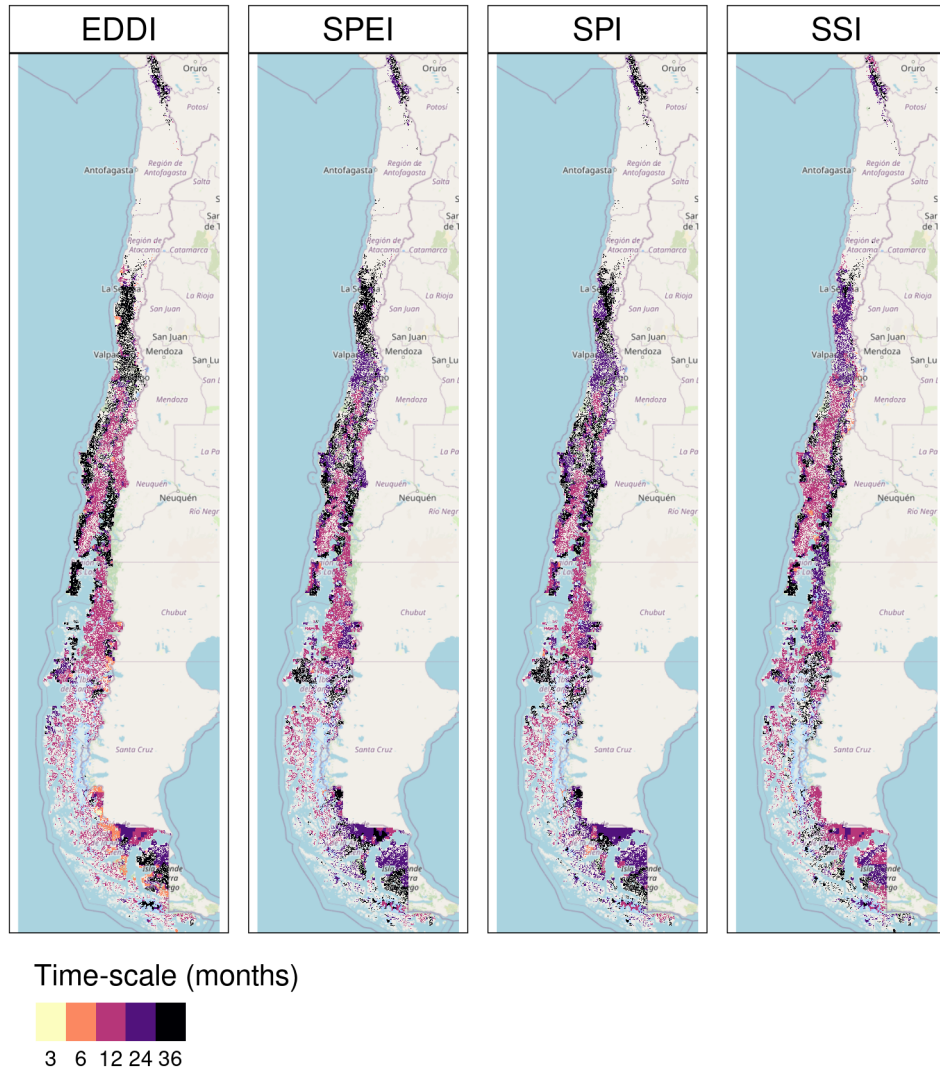


Figure 7: Time scales per drought index that reach the maximum coefficient of determination

the northern part of “Austral.” The SPI and SPEI have similar results, with the higher values in “Norte Chico” and “Centro” being higher than 0.6. Following a similar spatial pattern as EDDI. The SSI showed to be the index that has a major spatial extension with a higher correlation. It has a similar correlation to SPI and SPEI for “Norte Chico” and “Sur,” but has improvements for “Sur.”

In Table 5, we aggregate per macrozone and landcover the correlation analysis presented in Figure 7 and Figure 8. According to what is shown, forests seem to be the most resistant to drought. Showing that only “Centro” is slightly ( $rsq = 0.25$ ) impacted by a 12-month soil moisture deficit (SSI-12). In the “Norte Chico” and to a lesser extent in the “Norte Grande,” it is evident that a SSI-12 with a  $rsq = 0.45$  and a decrease in water supply (SPI-36 and SPEI-24 with  $rsq = 0.28$  and 0.34, respectively) have an impact on grasslands. However, this type was unaffected by soil moisture, water supply, or demand in macrozones further south. The types that show to be most affected by variation in climate conditions are shrublands, savannas, and croplands. For savannas in “Norte Chico,” the SSI-12 and SPI-24 reached an  $rsq$  of 0.74 and 0.58, respectively. This value decreases to the south, but the SSI-12 is still the variable explaining more of the variation in vegetation productivity ( $rsq = 0.45$  in “Centro” and 0.2 in “Sur”). In the case

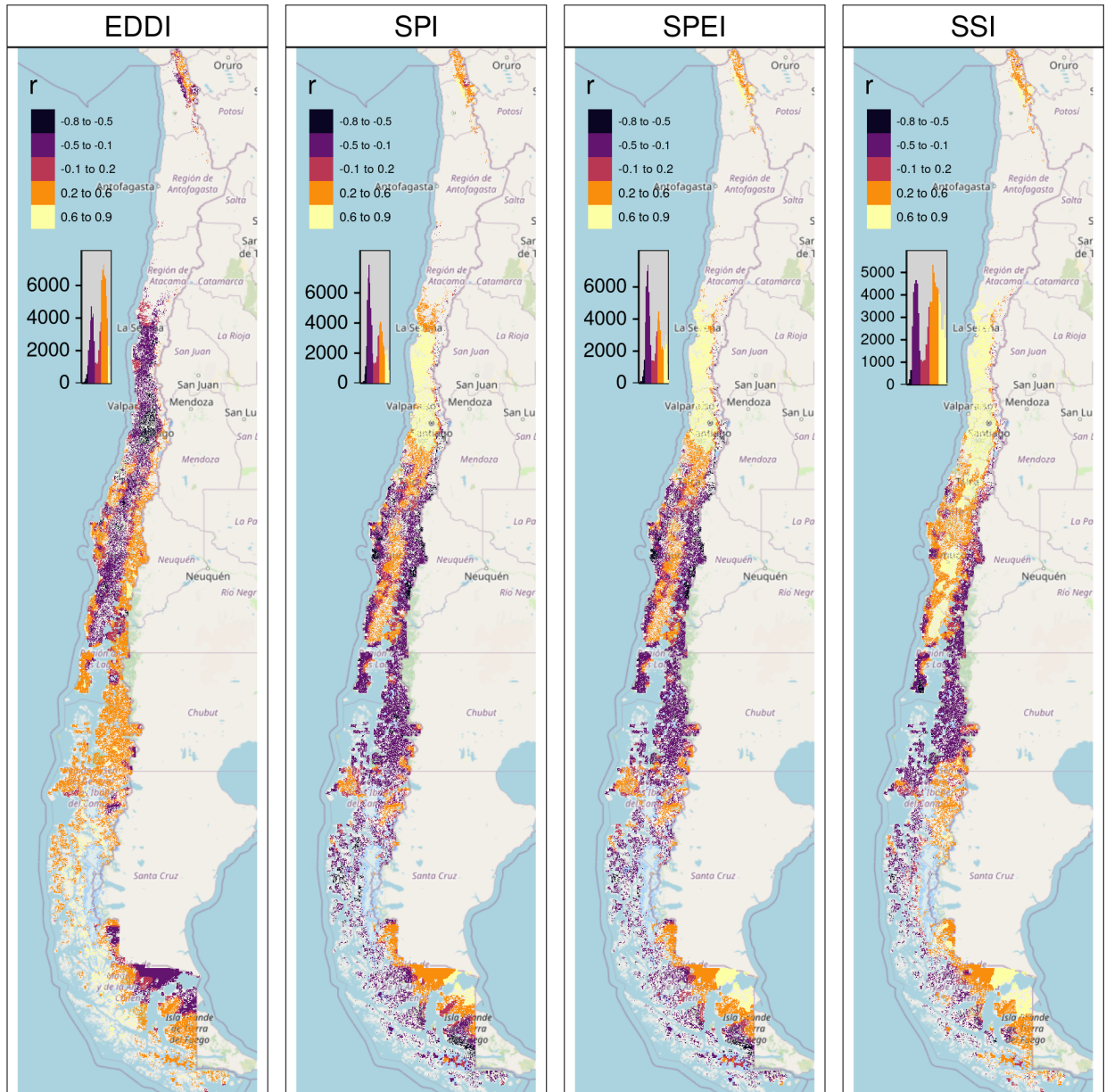


Figure 8: Pearson correlation value for the time scales and drought index that reach the maximum coefficient of determination

of croplands, the SPEI-12, SPI-36, and SSI-12 explain between 45% and 66% of the variability in “Norte Chico.” The type of land most impacted by climatic variation was shrubland, where soil moisture explained 59% and precipitation, 37%, in “Norte Chico” and “Centro,” with SSI-12 being the most relevant variable, then SPI-36 in “Norte Chico” and SPI-24 in “Sur.”

## 5. Discussion

### 5.1. Drought trend and attribution to land cover

Vicente-Serrano et al. (2022), in a study at the global scale of drought trends, indicate that there have not been significant trends in meteorological drought since 1950. Also, state that the increase in hidrological

Table 5: Summary per land cover macroclass and macrozone regarding the correlation between zcNDVI with the drought indices EDDI, SPI, SPEI, and SSI for time scales of 1, 3, 6, 12, 24, and 36. The numbers in each cell indicate the time scale that reached the maximum correlation for the land cover and macrozone, and the color indicates the strength of the r-squared obtained with the index and the time scale.

	Forest				Cropland				Grassland				Savanna				Shrubland			
macrozone	EDDI	SPI	SPEI	SSI	EDDI	SPI	SPEI	SSI	EDDI	SPI	SPEI	SSI	EDDI	SPI	SPEI	SSI	EDDI	SPI	SPEI	SSI
Norte Grande									36	36	36	12					36	12	36	12
Norte Chico					36	36	12	12	36	36	24	12	36	24	24	12	36	36	24	12
Centro	36	36	12	6	12	12	6	6	12	12	12	36	12	12	12	36	24	24	12	
Sur	36				6	6	6	6	6	6	6	12	6	6	6	6				
Austral	6	6									6	12	12	6	6	12				
 r-squared																				
0.2	0.4	0.6																		

trend in some parts of the globe (northeast Brazil and the Mediterranean region) is related to changes in land cover and specifically to the rapidly increasing irrigated area, which consequently increases water extraction. Kogan et al. (2020) analyzed the agricultural drought impact globally and in the main grain producer countries, finding that “since 1980, the Earth warming has not changed the drought area or intensity.” In our study, we considered the variation in vegetation productivity in Chile for areas without changes in land cover, to avoid misleading conclusions that could be related to the increase in water demand due to land cover change. Our results show a contrasting perspective. There has been a significant trend in the decline of vegetation productivity (zcNDVI) since 2000 for “Norte Chico” and “Centro,” which has been extreme between 2020 and 2022, seemingly due to an intense hydrological drought due to the persistence of the mega drought (Garreaud et al., 2017). However, a rise in irrigated land doesn’t seem to have an impact on this hydrological drought. Despite using the persistence mask for vegetation’s trend analysis, cropland, which is the most water-demand type, showed a decrease trend in “Norte Chico” and “Centro.” Also, there was an increase in barren land for both types. These changes are associated with a decrease in water demand from vegetation. Nonetheless, we used the persistent land cover to ensure that the pixel has the same class; in the case of croplands, it could happen that some areas had changed crops for others with higher water consumption and consequently increase water demand. But this effect should be minor compared to the results from land cover change at this scale of analysis.

On the other hand, for “Norte Chico” and “Centro,” our results show a decrease in trends of water supply (SPI and SSI), which are higher at larger time scales, which is evidence of the hydrological drought. We say that what happened in central Chile goes against what has been found on a global scale (Vicente-Serrano et al., 2022; Kogan et al., 2020). This shows that the main cause of the hydrological drought in Chile was a steady drop in water supply made worse by an increase in AED, but it seems that in zones most affected by drought, the main cause is not an increase in water demand by vegetation like irrigated crops. Finally, north-central Chile has experienced a decline in vegetation productivity across all macroclasses, which is primarily attributable to variations in water supply and soil moisture. An increase in water demand, such as an increase in the surface area of irrigated crops, could strengthen this trend.

## 5.2. Land cover types and their impact by drought

We discovered that croplands, savannas, and shrubland are the most susceptible to climatic changes and are most affected by the 12-month soil moisture deficit. In a study in the Yangtze River Basin in China, Jiang et al. (2020) analyzed the impact of drought on vegetation using the SPEI and the Enhanced Vegetation Index (EVI). They found that cropland was more sensitive to drought than grassland, showing that cropland

407 responds strongly to short- and medium-term drought (< SPEI-6). In our case, the SPEI-12 was the one that  
408 most impacted the croplands in “Norte Chico” and “Centro.” In general, most studies show that croplands  
409 are most sensitive to short-term drought (< SPI-6) (Zambrano et al., 2016; Potopová et al., 2015; Dai et al.,  
410 2020; Rhee et al., 2010). Short-term precipitation deficits impact soil water, and thus less water is available  
411 for plant growth. However, we found that in “Norte Chico,” an SPI-36 and SPEI-12 had a higher impact,  
412 which are associated with hydrological drought (long-term), and in “Centro,” an SPI-12 and SPEI-12. Thus,  
413 we attribute this impact to the hydrological drought that has decreased groundwater storage (Taucare et al.,  
414 2024), which in turn is impacted by long-term deficits, and consequently, the vegetation is more dependent on  
415 groundwater. In “Sur” and “Austral,” the correlations between drought indices and vegetation productivity  
416 decrease, as do the time scales that reach the maximum r-squared. What can be explained is that, south of  
417 “Centro,” predominate forest and grassland, the most resistant types. Also, drought episodes have been less  
418 frequent and intense. The drought episodes have had a lower impact on water availability for vegetation.

419 According to Senf et al. (2020), severe drought conditions in Europe are a significant cause of tree mortality.  
420 However, we found that forest is the type of land cover macroclass less affected by variation in drought indices,  
421 being the most resistant land cover class to drought. Supporting this is Fathi-Taperasht et al. (2022)], who  
422 assert that Indian forests are the most drought-resistant and recover rapidly. Similarly, the work of Wu  
423 et al. (2024), who analyzed vegetation loss and recovery in response to meteorological drought in the humid  
424 subtropical Pearl River basin in China, indicates that forests showed higher drought resistance. Using  
425 Vegetation Optical Depth (VOD), kNDVI, and EVI, Xiao et al. (2023) test the resistance of ecosystems  
426 and find that ecosystems with more forests are better able to handle severe droughts than croplands. They  
427 attribute the difference to a deeper rooting depth of trees, a higher water storage capacity, and different  
428 water use strategies between forest and cropland (Xiao et al., 2023).

429 In contrast to what we obtained, Venegas-González et al. (2023), who studied *Cryptocarya alba* and  
430 *Beilschmiedia miersii* (both from the Lauraceae family) that live in sclerophyllous forests in Chile, found  
431 that the trees’ overall growth had slowed down. This could mean that the natural dynamics of their forests  
432 have changed. They attributed it to the cumulative effects of the unprecedented drought (i.e., hydrological  
433 drought). Thus, we attribute that forest to being the most resistant to drought, due to the fact that most  
434 of the species comprising it are highly resilient to water scarcity compared to the other land cover classes.  
435 Nonetheless, if we want to go deep in our analysis, we should use earth observation data that is able to  
436 capture a higher level of detail. For example, when we used MOD13A3 with a 1km spatial resolution to  
437 measure vegetation condition, it took the average condition of 1 square kilometer. Then, to use remote  
438 sensing to look at how a certain type of forest (like sclerophyllous forest) changes in response to drought on  
439 a local level, we should use operational products with higher spatial resolutions, like those from Landsat or  
440 Sentinel. This will let us do a more thorough analysis.

#### 441 5.3. Soil moisture, vegetation productivity, and agricultural drought.

442 The main external factors that affect biomass production by vegetation are actual evapotranspiration and  
443 soil moisture, and the rate of ET in turn depends on the availability of water storage in the root zone.  
444 Thus, soil moisture plays a key role in land carbon uptake and, consequently, in the production of biomass  
445 (Humphrey et al., 2021). Moreover, Zhang et al. (2022) indicate there is a bidirectional causality between  
446 soil moisture and vegetation productivity. Lastly, some studies have redefined agricultural drought as soil  
447 moisture drought from a hydrological perspective (Van Loon et al., 2016; Samaniego et al., 2018). Even  
448 though soil moisture is the external factor most determinant of vegetation biomass, there are multiple internal  
449 factors, such as species, physiological characteristics, and plant hydraulics, that would affect vegetation  
450 productivity. Because of that, we believe that agricultural drought, referring to the drought that impacts  
451 vegetation productivity, is the most proper term, as originally defined by Wilhite and Glantz (1985).

452 The study results showed that the soil moisture-based drought index (SSI) was better at explaining vegeta-  
453 tion productivity across land cover macroclasses than meteorological drought indices like SPI, SPEI, and  
454 EDDI. In the early growing season and especially in irrigated rather than rainfed croplands, soil moisture  
455 has better skills than SPI and SPEI for estimating gross primary production (GPP). This according to

456 Chatterjee et al. (2022) evaluation of the SPI and SPEI and their correlation with GPP in the CONUS.  
457 Also, Zhou et al. (2021) indicate that the monthly scaled Standardized Water Deficit Index (SWDI) can  
458 accurately show the effects of agricultural drought in most of China. Nicolai-Shaw et al. (2017) also looked  
459 at the time-lag between the SWDI and the Vegetation Condition Index (VCI). They found that there was  
460 little to no time-lag in croplands but a greater time-lag in forests.

461 In our case, there is strong spatial variability throughout Chile and between classes, mainly attributable to  
462 climate heterogeneity, hydrological status, or vegetation resistance to water scarcity. The semi-arid “Norte  
463 Chico” and the Mediterranean “Centro” were where SSI had the best performance. In Chile, medium-term  
464 deficits of 12 months are more relevant in the response of vegetation, which decreases to the south, and in the  
465 case of croplands, they seem to react in a shorter time, with six months (SSI-6) in “Centro.” This variation  
466 for croplands could be related to the fact that in “Norte Chico,” the majority of crops are irrigated, but  
467 to the south there is a higher proportion of rainfed agriculture, which is most dependent on the short-term  
468 availability of water. Rather, in the “Norte Chico,” the orchards are more dependent on the storage of water  
469 in dams of groundwater reservoirs, which are affected by long-term drought (e.g., SPI-36).

#### 470 5.4. Future outlook (to complete)

## 471 6. Conclusion

472 There is a trend toward decreasing water supply in most parts of Chile, particularly in the “Centro” and  
473 “Norte Chico” regions. The whole country showed an increase in AED. Vegetation productivity only showed  
474 a decrease in the “Norte Chico” and “Centro,” being highest for shrubland and croplands. Forest is the land  
475 cover most resistant to drought, as shown along Chile, and shrubland and cropland are the most sensitive.

476 A soil moisture deficit of 12 months (SSI-12) is highly correlated with vegetation productivity for the land  
477 cover classes of shrubland, savannas, croplands, and forest in “Norte Chico” and “Centro.” For the southern  
478 part of the country with humid conditions, the correlation with SSI decreases. Soil moisture overcomes  
479 the capacity to explain vegetation productivity over the supply and demand drought indices in the entire  
480 territory.

481 The variation in vegetation productivity appears to be associated with climate variation rather than an-  
482 thropogenic factors (e.g., an increase in water demand by irrigated crops). Even though switching to more  
483 demanding crops on the land could increase the impact of drought on vegetation, this would need to be  
484 more thoroughly investigated, for instance at the watershed level.

485 The results of this study could help in the development of a robust forecasting system for land cover classes  
486 in Chile, helping to improve preparedness for climate change impacts on vegetation.

## 487 Supplementary material

## 488 References

- 489 Abramowitz, M., Stegun, I.A., 1968. Handbook of mathematical functions with formulas, graphs, and mathematical tables.  
490 volume 55. US Government printing office.
- 491 Aceituno, P., Boisier, J.P., Garreaud, R., Rondanelli, R., Rutllant, J.A., 2021. Climate and Weather in Chile, in: Fernández,  
492 B., Gironás, J. (Eds.), Water Resources of Chile. Springer International Publishing, Cham. volume 8, pp. 7–29. URL:  
493 [http://link.springer.com/10.1007/978-3-030-56901-3\\_2](http://link.springer.com/10.1007/978-3-030-56901-3_2).
- 494 AghaKouchak, A., 2014. A baseline probabilistic drought forecasting framework using standardized soil moisture in-  
495 dex: application to the 2012 United States drought. Hydrology and Earth System Sciences 18, 2485–2492. URL:  
496 <https://hess.copernicus.org/articles/18/2485/2014/>, doi:10.5194/hess-18-2485-2014.
- 497 AghaKouchak, A., Mirchi, A., Madani, K., Di Baldassarre, G., Nazemi, A., Alborzi, A., Anjileli, H., Azarderakhsh, M., Chiang,  
498 F., Hassanzadeh, E., Huning, L.S., Mallakpour, I., Martinez, A., Mazdiyasni, O., Moftakhari, H., Norouzi, H., Sadegh,  
499 M., Sadeqi, D., Van Loon, A.F., Wanders, N., 2021. Anthropogenic Drought: Definition, Challenges, and Opportuni-  
500 ties. Reviews of Geophysics 59, e2019RG000683. URL: <https://agupubs.onlinelibrary.wiley.com/doi/10.1029/2019RG000683>,  
501 doi:10.1029/2019RG000683.
- 502 Akinyemi, F.O., 2021. Vegetation Trends, Drought Severity and Land Use-Land Cover Change during the Growing Season in  
503 Semi-Arid Contexts. Remote Sensing 2021, Vol. 13, Page 836 13, 836. URL: <https://www.mdpi.com/2072-4292/13/5/836/>  
504 htm, doi:10.3390/RS13050836. publisher: Multidisciplinary Digital Publishing Institute.

- 505 Bakker, K., 2012. Water Security: Research Challenges and Opportunities. *Science* 337, 914–915. URL: <https://www.science.org/doi/10.1126/science.1226337>, doi:[10.1126/science.1226337](https://doi.org/10.1126/science.1226337).
- 506 Beck, H.E., McVicar, T.R., Vergopolan, N., Berg, A., Lutsko, N.J., Dufour, A., Zeng, Z., Jiang, X., van Dijk, A.I.J.M., Miralles, D.G., 2023. High-resolution (1 km) Köppen-Geiger maps for 1901–2099 based on constrained CMIP6 projections. *Scientific Data* 10. URL: <http://dx.doi.org/10.1038/s41597-023-02549-6>, doi:[10.1038/s41597-023-02549-6](https://doi.org/10.1038/s41597-023-02549-6).
- 507 Beguería, S., Vicente-Serrano, S.M., 2023. SPEI: Calculation of the Standardized Precipitation-Evapotranspiration Index. URL: <https://CRAN.R-project.org/package=SPEI>.
- 508 Boisier, J.P., Alvarez-Garreton, C., Cordero, R.R., Damiani, A., Gallardo, L., Garreaud, R.D., Lambert, F., Ramallo, C., Rojas, M., Rondanelli, R., 2018. Anthropogenic drying in central-southern Chile evidenced by long-term observations and climate model simulations. *Elementa* 6, 74. URL: <https://www.elementascience.org/article/10.1525/elementa.328/>, doi:[10.1525/elementa.328](https://doi.org/10.1525/elementa.328).
- 509 Calvin, K., Dasgupta, D., Krinner, G., Mukherji, A., Thorne, P.W., Trisos, C., Romero, J., Aldunce, P., Barrett, K., Blanco, G., Cheung, W.W., Connors, S., Denton, F., Diongue-Niang, A., Dodman, D., Garschagen, M., Geden, O., Hayward, B., Jones, C., Jotzo, F., Krug, T., Lasco, R., Lee, Y.Y., Masson-Delmotte, V., Meinshausen, M., Mintenbeck, K., Mokssit, A., Otto, F.E., Pathak, M., Pirani, A., Poloczanska, E., Pörtner, H.O., Revi, A., Roberts, D.C., Roy, J., Ruane, A.C., Skea, J., Shukla, P.R., Slade, R., Slangen, A., Sokona, Y., Sörensson, A.A., Tignor, M., Van Vuuren, D., Wei, Y.M., Winkler, H., Zhai, P., Zommers, Z., Hourcade, J.C., Johnson, F.X., Pachauri, S., Simpson, N.P., Singh, C., Thomas, A., Totin, E., Arias, P., Bustamante, M., Elgizouli, I., Flato, G., Howden, M., Méndez-Vallejo, C., Pereira, J.J., Pichs-Madruga, R., Rose, S.K., Saheb, Y., Sánchez Rodríguez, R., Ürge Vorsatz, D., Xiao, C., Yassaa, N., Alegría, A., Armour, K., Bednar-Friedl, B., Blok, K., Cissé, G., Dentener, F., Eriksen, S., Fischer, E., Garner, G., Guiavarch, C., Haasnoot, M., Hansen, G., Hauser, M., Hawkins, E., Hermans, T., Kopp, R., Leprince-Ringuet, N., Lewis, J., Ley, D., Ludden, C., Niamir, L., Nicholls, Z., Some, S., Szopa, S., Trewin, B., Van Der Wijst, K.I., Winter, G., Witting, M., Birt, A., Ha, M., Romero, J., Kim, J., Haites, E.F., Jung, Y., Stavins, R., Birt, A., Ha, M., Orendain, D.J.A., Ignon, L., Park, S., Park, Y., Reisinger, A., Cammaramo, D., Fischlin, A., Fuglestvedt, J.S., Hansen, G., Ludden, C., Masson-Delmotte, V., Matthews, J.R., Mintenbeck, K., Pirani, A., Poloczanska, E., Leprince-Ringuet, N., Péan, C., 2023. IPCC, 2023: Climate Change 2023: Synthesis Report. Contribution of Working Groups I, II and III to the Sixth Assessment Report of the Intergovernmental Panel on Climate Change [Core Writing Team, H. Lee and J. Romero (eds.)]. IPCC, Geneva, Switzerland. Technical Report. Intergovernmental Panel on Climate Change (IPCC). URL: <https://www.ipcc.ch/report/ar6/syr/>.
- 510 Chamling, M., Bera, B., 2020. Spatio-temporal Patterns of Land Use/Land Cover Change in the Bhutan–Bengal Foothill Region Between 1987 and 2019: Study Towards Geospatial Applications and Policy Making. *Earth Systems and Environment* 4, 117–130. URL: <http://link.springer.com/10.1007/s41748-020-00150-0>, doi:[10.1007/s41748-020-00150-0](https://doi.org/10.1007/s41748-020-00150-0).
- 511 Chatterjee, S., Desai, A.R., Zhu, J., Townsend, P.A., Huang, J., 2022. Soil moisture as an essential component for delineating and forecasting agricultural rather than meteorological drought. *Remote Sensing of Environment* 269, 112833. URL: <https://linkinghub.elsevier.com/retrieve/pii/S0034425721005538>, doi:[10.1016/j.rse.2021.112833](https://doi.org/10.1016/j.rse.2021.112833).
- 512 Chen, J., Shao, Z., Huang, X., Zhuang, Q., Dang, C., Cai, B., Zheng, X., Ding, Q., 2022. Assessing the impact of drought-land cover change on global vegetation greenness and productivity. *Science of The Total Environment* 852, 158499. URL: <https://linkinghub.elsevier.com/retrieve/pii/S004896972205598X>, doi:[10.1016/j.scitotenv.2022.158499](https://doi.org/10.1016/j.scitotenv.2022.158499).
- 513 Crausbay, S.D., Ramirez, A.R., Carter, S.L., Cross, M.S., Hall, K.R., Bathke, D.J., Betancourt, J.L., Colt, S., Cravens, A.E., Dalton, M.S., Dunham, J.B., Hay, L.E., Hayes, M.J., McEvoy, J., McNutt, C.A., Moritz, M.A., Nislow, K.H., Raheem, N., Sanford, T., 2017. Defining Ecological Drought for the Twenty-First Century. *Bulletin of the American Meteorological Society* 98, 2543–2550. URL: <https://journals.ametsoc.org/view/journals/bams/98/12/bams-d-16-0292.1.xml>, doi:[10.1175/BAMS-D-16-0292.1](https://doi.org/10.1175/BAMS-D-16-0292.1). publisher: American Meteorological Society.
- 514 Dai, M., Huang, S., Huang, Q., Leng, G., Guo, Y., Wang, L., Fang, W., Li, P., Zheng, X., 2020. Assessing agricultural drought risk and its dynamic evolution characteristics. *Agricultural Water Management* 231, 106003. URL: <https://linkinghub.elsevier.com/retrieve/pii/S0378377419316531>, doi:[10.1016/j.agwat.2020.106003](https://doi.org/10.1016/j.agwat.2020.106003).
- 515 Didan, K., 2015. MOD13Q1 MODIS/Terra Vegetation Indices 16-Day L3 Global 250m SIN Grid V006. Technical Report. NASA EOSDIS Land Processes DAAC. doi:[http://dx.doi.org/10.5067/MODIS/MOD13Q1.006](https://dx.doi.org/10.5067/MODIS/MOD13Q1.006).
- 516 Farahmand, A., AghaKouchak, A., 2015. A generalized framework for deriving nonparametric standardized drought indicators. *Advances in Water Resources* 76, 140–145. URL: <https://linkinghub.elsevier.com/retrieve/pii/S0309170814002322>, doi:[10.1016/j.advwatres.2014.11.012](https://doi.org/10.1016/j.advwatres.2014.11.012).
- 517 Fathi-Taperasht, A., Shafizadeh-Moghadam, H., Minaei, M., Xu, T., 2022. Influence of drought duration and severity on drought recovery period for different land cover types: evaluation using MODIS-based indices. *Ecological Indicators* 141, 109146. URL: <https://linkinghub.elsevier.com/retrieve/pii/S1470160X22006185>, doi:[10.1016/j.ecolind.2022.109146](https://doi.org/10.1016/j.ecolind.2022.109146).
- 518 Ford, T.W., Otkin, J.A., Quiring, S.M., Lisonbee, J., Woloszyn, M., Wang, J., Zhong, Y., 2023. Flash Drought Indicator Intercomparison in the United States. *Journal of Applied Meteorology and Climatology* 62, 1713–1730. URL: <https://journals.ametsoc.org/view/journals/apme/62/12/JAMC-D-23-0081.1.xml>, doi:[10.1175/JAMC-D-23-0081.1](https://doi.org/10.1175/JAMC-D-23-0081.1).
- 519 Fuentes, I., Fuster, R., Avilés, D., Vervoort, W., 2021. Water scarcity in central Chile: the effect of climate and land cover changes on hydrologic resources. *Hydrological Sciences Journal* 66, 1028–1044. URL: <https://www.tandfonline.com/doi/full/10.1080/02626667.2021.1903475>, doi:[10.1080/02626667.2021.1903475](https://doi.org/10.1080/02626667.2021.1903475).
- 520 Garreaud, R., Alvarez-Garreton, C., Barichivich, J., Boisier, J.P., Christie, D., Galleguillos, M., LeQuenne, C., McPhee, J., Zambrano-Bigiarini, M., 2017. The 2010–2015 mega drought in Central Chile: Impacts on regional hydroclimate and vegetation. *Hydrology and Earth System Sciences Discussions* 2017, 1–37. URL: <http://www.hydrol-earth-syst-sci-discuss.net/hess-2017-191/>, doi:[10.5194/hess-2017-191](https://doi.org/10.5194/hess-2017-191).
- 521 Garreaud, R.D., 2009. The Andes climate and weather. *Advances in Geosciences* 22, 3–11. URL: <https://adgeo.copernicus.org/articles/22/3/2009/>, doi:[10.5194/adgeo-22-3-2009](https://doi.org/10.5194/adgeo-22-3-2009).

- 570 Gebrechorkos, S.H., Peng, J., Dyer, E., Miralles, D.G., Vicente-Serrano, S.M., Funk, C., Beck, H.E., Asfaw, D.T., Singer, M.B.,  
 571 Dadson, S.J., 2023. Global high-resolution drought indices for 1981–2022. *Earth System Science Data* 15, 5449–5466. URL:  
 572 <https://essd.copernicus.org/articles/15/5449/2023/>, doi:10.5194/essd-15-5449-2023.
- 573 Hao, Z., AghaKouchak, A., 2013. Multivariate Standardized Drought Index: A parametric multi-index model. *Advances in Water Resources* 57, 12–18. URL: <https://linkinghub.elsevier.com/retrieve/pii/S0309170813000493>, doi:10.1016/j.advwatres.2013.03.009.
- 574 Hargreaves, G.H., 1994. Defining and Using Reference Evapotranspiration. *Journal of Irrigation and Drainage Engineering* 120,  
 575 1132–1139. URL: <https://ascelibrary.org/doi/10.1061/%28ASCE%290733-9437%281994%29120%3A6%281132%29>, doi:10.  
 576 1061/(ASCE)0733-9437(1994)120:6(1132).
- 577 Hargreaves, G.H., Samani, Z.A., 1985. Reference crop evapotranspiration from temperature. *Applied engineering in agriculture*  
 578 1, 96–99.
- 579 Heim, R.R., 2002. A Review of Twentieth-Century Drought Indices Used in the United States. *Bulletin of the American  
 580 Meteorological Society* 83, 1149–1166. URL: <https://journals.ametsoc.org/doi/10.1175/1520-0477-83.8.1149>, doi:10.1175/  
 581 1520-0477-83.8.1149.
- 582 Hijmans, R.J., 2023. terra: Spatial Data Analysis. URL: <https://CRAN.R-project.org/package=terra>.
- 583 Hobbins, M.T., Wood, A., McEvoy, D.J., Huntington, J.L., Morton, C., Anderson, M., Hain, C., 2016. The Evaporative Demand  
 584 Drought Index. Part I: Linking Drought Evolution to Variations in Evaporative Demand. *Journal of Hydrometeorology* 17,  
 585 1745–1761. URL: <http://journals.ametsoc.org/doi/10.1175/JHM-D-15-0121.1>, doi:10.1175/JHM-D-15-0121.1.
- 586 Homer, C., Dewitz, J., Jin, S., Xian, G., Costello, C., Danielson, P., Gass, L., Funk, M., Wickham, J., Stehman, S., Auch, R.,  
 587 Riitters, K., 2020. Conterminous United States land cover change patterns 2001–2016 from the 2016 National Land Cover  
 588 Database. *ISPRS Journal of Photogrammetry and Remote Sensing* 162, 184–199. URL: <https://linkinghub.elsevier.com/retrieve/pii/S0924271620300587>, doi:10.1016/j.isprsjprs.2020.02.019.
- 589 Hufkens, K., Stauffer, R., Campitelli, E., 2019. The ecwmfr package: an interface to ECMWF API endpoints. URL: <https://bluegreen-labs.github.io/ecwmfr/>.
- 590 Humphrey, V., Berg, A., Ciais, P., Gentile, P., Jung, M., Reichstein, M., Seneviratne, S.I., Frankenberg, C., 2021. Soil  
 591 moisture–atmosphere feedback dominates land carbon uptake variability. *Nature* 592, 65–69. URL: <https://www.nature.com/articles/s41586-021-03325-5>, doi:10.1038/s41586-021-03325-5.
- 592 IPCC, 2013. Climate Change 2013: The Physical Science Basis. Contribution of Working Group I to the Fifth Assessment  
 593 Report of the Intergovernmental Panel on Climate Change. Cambridge University Press, Cambridge, UK; New York, USA.  
 594 URL: [www.climatechange2013.org](http://www.climatechange2013.org), doi:10.1017/CBO9781107415324.
- 595 Jiang, W., Wang, L., Feng, L., Zhang, M., Yao, R., 2020. Drought characteristics and its impact on changes in surface  
 596 vegetation from 1981 to 2015 in the Yangtze River Basin, China. *International Journal of Climatology* 40, 3380–3397. URL:  
 597 <https://rmets.onlinelibrary.wiley.com/doi/10.1002/joc.6403>, doi:10.1002/joc.6403.
- 598 Kendall, M., 1975. Rank correlation methods (4th ed. 2d impression). Griffin.
- 599 Kogan, F., Guo, W., Yang, W., 2020. Near 40-year drought trend during 1981–2019 earth warming and food security. *Geomatics,  
 600 Natural Hazards and Risk* 11, 469–490. URL: <https://www.tandfonline.com/doi/full/10.1080/19475705.2020.1730452>, doi:10.1080/19475705.2020.1730452.
- 601 Kuhn, M., Wickham, H., 2020. Tidymodels: a collection of packages for modeling and machine learning using tidyverse  
 602 principles. URL: <https://www.tidymodels.org>.
- 603 Laimighofer, J., Laaha, G., 2022. How standard are standardized drought indices? Uncertainty components for the SPI  
 604 & SPEI case. *Journal of Hydrology* 613, 128385. URL: <https://linkinghub.elsevier.com/retrieve/pii/S0022169422009544>, doi:10.1016/j.jhydrol.2022.128385.
- 605 Li, H., Choy, S., Zaminpardaz, S., Wang, X., Liang, H., Zhang, K., 2024. Flash drought monitoring using diurnal-provided  
 606 evaporative demand drought index. *Journal of Hydrology* 633, 130961. URL: <https://linkinghub.elsevier.com/retrieve/pii/S002216942400355X>, doi:10.1016/j.jhydrol.2024.130961.
- 607 Li, W., Migliavacca, M., Forkel, M., Denissen, J.M.C., Reichstein, M., Yang, H., Duveiller, G., Weber, U., Orth, R., 2022.  
 608 Widespread increasing vegetation sensitivity to soil moisture. *Nature Communications* 13, 3959. URL: <https://www.nature.com/articles/s41467-022-31667-9>, doi:10.1038/s41467-022-31667-9.
- 609 Liu, X., Yu, S., Yang, Z., Dong, J., Peng, J., 2024. The first global multi-timescale daily SPEI dataset from 1982 to 2021.  
 610 *Scientific Data* 11, 223. URL: <https://www.nature.com/articles/s41597-024-03047-z>, doi:10.1038/s41597-024-03047-z.
- 611 Luebert, F., Pliscott, P., 2022. The vegetation of Chile and the EcoVeg approach in the context of the International Vegetation  
 612 Classification project. *Vegetation Classification and Survey* 3, 15–28. URL: <https://vcs.pensoft.net/article/67893/>, doi:10.  
 613 3897/VCS.67893.
- 614 Luo, L., Apps, D., Arcand, S., Xu, H., Pan, M., Hoerling, M., 2017. Contribution of temperature and precipitation anomalies to  
 615 the California drought during 2012–2015. *Geophysical Research Letters* 44, 3184–3192. URL: <https://agupubs.onlinelibrary.wiley.com/doi/10.1002/2016GL072027>, doi:10.1002/2016GL072027.
- 616 Luyssaert, S., Jammet, M., Stoy, P.C., Estel, S., Pongratz, J., Ceschia, E., Churkina, G., Don, A., Erb, K., Ferlicoq, M.,  
 617 Gielen, B., Grünwald, T., Houghton, R.A., Klumpp, K., Knohl, A., Kolb, T., Kuemmerle, T., Laurila, T., Lohila, A.,  
 618 Loustau, D., McGrath, M.J., Meyfroidt, P., Moors, E.J., Naudts, K., Novick, K., Otto, J., Pilegaard, K., Pio, C.A., Rambal,  
 619 S., Rebmann, C., Ryder, J., Suyker, A.E., Varlagin, A., Wattenbach, M., Dolman, A.J., 2014. Land management and  
 620 land-cover change have impacts of similar magnitude on surface temperature. *Nature Climate Change* 4, 389–393. URL:  
 621 <https://www.nature.com/articles/nclimate2196>, doi:10.1038/nclimate2196.
- 622 Masson-Delmotte, V., P.Z.A.P.S.L.C.C.P.S.B.N.C.Y.C.L.G.M.I.G.M.H.K.L.E.L.J.B.R.M.T.K.M.T.W.O.Y.R.Y.a.B.Z.e., 2021.  
 623 IPCC, 2021: Climate Change 2021: The Physical Science Basis. Contribution of Working Group I to the Sixth Assessment  
 624 Report of the Intergovernmental Panel on Climate Change. Technical Report. URL: <https://www.ipcc.ch/>. publication

- 635        Title: Cambridge University Press. In Press.
- 636        McEvoy, D.J., Huntington, J.L., Hobbins, M.T., Wood, A., Morton, C., Anderson, M., Hain, C., 2016. The Evaporative Demand  
 637        Drought Index. Part II: CONUS-Wide Assessment against Common Drought Indicators. *Journal of Hydrometeorology* 17,  
 638        1763–1779. URL: <http://journals.ametsoc.org/doi/10.1175/JHM-D-15-0122.1>, doi:[10.1175/JHM-D-15-0122.1](https://doi.org/10.1175/JHM-D-15-0122.1).
- 639        Meroni, M., Rembold, F., Fasbender, D., Vrieling, A., 2017. Evaluation of the Standardized Precipitation Index as an early  
 640        predictor of seasonal vegetation production anomalies in the Sahel. *Remote Sensing Letters* 8, 301–310. URL: <http://www.tandfonline.com/doi/abs/10.1080/2150704X.2016.1264020>, doi:[10.1080/2150704X.2016.1264020](https://doi.org/10.1080/2150704X.2016.1264020).
- 641        Miranda, A., Lara, A., Altamirano, A., Di Bella, C., González, M.E., Julio Camarero, J., 2020. Forest browning trends in  
 642        response to drought in a highly threatened mediterranean landscape of South America. *Ecological Indicators* 115, 106401.  
 643        URL: <https://linkinghub.elsevier.com/retrieve/pii/S1470160X20303381>, doi:[10.1016/j.ecolind.2020.106401](https://doi.org/10.1016/j.ecolind.2020.106401).
- 644        Miranda, A., Syphard, A.D., Berdugo, M., Carrasco, J., Gómez-González, S., Ovalle, J.F., Delpiano, C.A., Vargas, S.,  
 645        Squeo, F.A., Miranda, M.D., Dobbs, C., Mentler, R., Lara, A., Garreaud, R., 2023. Widespread synchronous decline  
 646        of Mediterranean-type forest driven by accelerated aridity. *Nature Plants* 9, 1810–1817. URL: <https://www.nature.com/articles/s41477-023-01541-7>, doi:[10.1038/s41477-023-01541-7](https://doi.org/10.1038/s41477-023-01541-7).
- 647        Muñoz-Sabater, J., Dutra, E., Agustí-Panareda, A., Albergel, C., Arduini, G., Balsamo, G., Boussetta, S., Choulga, M.,  
 648        Harrigan, S., Hersbach, H., Martens, B., Miralles, D.G., Piles, M., Rodríguez-Fernández, N.J., Zsoter, E., Buontempo, C.,  
 649        Thépaut, J.N., 2021. ERA5-Land: a state-of-the-art global reanalysis dataset for land applications. *Earth System Science  
 650        Data* 13, 4349–4383. URL: <https://essd.copernicus.org/articles/13/4349/2021/>, doi:[10.5194/essd-13-4349-2021](https://doi.org/10.5194/essd-13-4349-2021).
- 651        Narasimhan, B., Srinivasan, R., 2005. Development and evaluation of Soil Moisture Deficit Index (SMDI) and Evapotranspi-  
 652        ration Deficit Index (ETDI) for agricultural drought monitoring. *Agricultural and Forest Meteorology* 133, 69–88. URL:  
 653        <https://linkinghub.elsevier.com/retrieve/pii/S0168192305001565>, doi:[10.1016/j.agrformet.2005.07.012](https://doi.org/10.1016/j.agrformet.2005.07.012).
- 654        Nicolai-Shaw, N., Zscheischler, J., Hirsch, M., Gudmundsson, L., Seneviratne, S.I., 2017. A drought event composite analysis  
 655        using satellite remote-sensing based soil moisture. *Remote Sensing of Environment* 203, 216–225. URL: [https://linkinghub.elsevier.com/retrieve/pii/S0034425717302729](https://linkinghub.<br/>
  656        elsevier.com/retrieve/pii/S0034425717302729), doi:[10.1016/j.rse.2017.06.014](https://doi.org/10.1016/j.rse.2017.06.014).
- 657        Noguera, I., Vicente-Serrano, S.M., Domínguez-Castro, F., 2022. The Rise of Atmospheric Evaporative Demand Is Increasing  
 658        Flash Droughts in Spain During the Warm Season. *Geophysical Research Letters* 49, e2021GL097703. URL: [https://agupubs.onlinelibrary.wiley.com/doi/10.1029/2021GL097703](https://agupubs.<br/>
  659        onlinelibrary.wiley.com/doi/10.1029/2021GL097703), doi:[10.1029/2021GL097703](https://doi.org/10.1029/2021GL097703).
- 660        Pebesma, E., 2018. Simple Features for R: Standardized Support for Spatial Vector Data. *The R Journal* 10, 439–446. URL:  
 661        <https://doi.org/10.32614/RJ-2018-009>, doi:[10.32614/RJ-2018-009](https://doi.org/10.32614/RJ-2018-009).
- 662        Pebesma, E., Bivand, R., 2023. Spatial Data Science: With applications in R. Chapman and Hall/CRC, London. URL:  
 663        <https://r-spatial.org/book/>.
- 664        Peng, D., Zhang, B., Wu, C., Huete, A.R., Gonsamo, A., Lei, L., Ponce-Campos, G.E., Liu, X., Wu, Y., 2017. Country-level  
 665        net primary production distribution and response to drought and land cover change. *Science of The Total Environment* 574,  
 666        65–77. URL: <https://linkinghub.elsevier.com/retrieve/pii/S0048969716319507>, doi:[10.1016/j.scitotenv.2016.09.033](https://doi.org/10.1016/j.scitotenv.2016.09.033).
- 667        Pitman, A.J., De Noblet-Ducoudré, N., Avila, F.B., Alexander, L.V., Boisier, J.P., Brovkin, V., Delire, C., Cruz, F., Donat,  
 668        M.G., Gayler, V., Van Den Hurk, B., Reick, C., Volodire, A., 2012. Effects of land cover change on temperature and  
 669        rainfall extremes in multi-model ensemble simulations. *Earth System Dynamics* 3, 213–231. URL: <https://esd.copernicus.org/articles/3/213/2012/>, doi:[10.5194/esd-3-213-2012](https://doi.org/10.5194/esd-3-213-2012).
- 670        Potopová, V., Stepánek, P., Mozný, M., Türkott, L., Soukup, J., 2015. Performance of the standarised precipitation evapotran-  
 671        spiration index at various lags for agricultural drought risk assessment in the {C}zech {R}epublic. *Agricultural and Forest  
 672        Meteorology* 202, 26–38.
- 673        R Core Team, 2023. R: A Language and Environment for Statistical Computing. R Foundation for Statistical Computing,  
 674        Vienna, Austria. URL: <https://www.R-project.org/>.
- 675        Rhee, J., Im, J., Carbone, G.J., 2010. Monitoring agricultural drought for arid and humid regions using multi-sensor remote  
 676        sensing data. *Remote Sensing of Environment* 114, 2875–2887. URL: <http://www.sciencedirect.com/science/article/pii/S003442571000221X>, doi:[10.1016/j.rse.2010.07.005](https://doi.org/10.1016/j.rse.2010.07.005).
- 677        Samaniego, L., Thober, S., Kumar, R., Wanders, N., Rakovec, O., Pan, M., Zink, M., Sheffield, J., Wood, E.F., Marx, A.,  
 678        2018. Anthropogenic warming exacerbates European soil moisture droughts. *Nature Climate Change* 8, 421–426. URL:  
 679        <https://www.nature.com/articles/s41558-018-0138-5>, doi:[10.1038/s41558-018-0138-5](https://doi.org/10.1038/s41558-018-0138-5).
- 680        Sen, P.K., 1968. Estimates of the Regression Coefficient Based on Kendall's Tau. *Journal of the American Statistical Association*  
 681        63, 1379–1389. URL: <http://www.tandfonline.com/doi/abs/10.1080/01621459.1968.10480934>, doi:[10.1080/01621459.1968.10480934](https://doi.org/10.1080/01621459.1968.10480934).
- 682        Senf, C., Buras, A., Zang, C.S., Rammig, A., Seidl, R., 2020. Excess forest mortality is consistently linked to drought  
 683        across Europe. *Nature Communications* 11, 6200. URL: <https://www.nature.com/articles/s41467-020-19924-1>, doi:[10.1038/s41467-020-19924-1](https://doi.org/10.1038/s41467-020-19924-1).
- 684        Slette, I.J., Post, A.K., Awad, M., Even, T., Punzalan, A., Williams, S., Smith, M.D., Knapp, A.K., 2019. How ecologists  
 685        define drought, and why we should do better. *Global Change Biology* 25, 3193–3200. URL: <https://onlinelibrary.wiley.com/doi/10.1111/gcb.14747>, doi:[10.1111/gcb.14747](https://doi.org/10.1111/gcb.14747).
- 686        Song, X.P., Hansen, M.C., Stehman, S.V., Potapov, P.V., Tyukavina, A., Vermote, E.F., Townshend, J.R., 2018. Global land  
 687        change from 1982 to 2016. *Nature* 560, 639–643. URL: <https://www.nature.com/articles/s41586-018-0411-9>, doi:[10.1038/s41586-018-0411-9](https://doi.org/10.1038/s41586-018-0411-9).
- 688        Souza, A.G.S.S., Ribeiro Neto, A., Souza, L.L.D., 2021. Soil moisture-based index for agricultural drought assessment: SMADI  
 689        application in Pernambuco State-Brazil. *Remote Sensing of Environment* 252, 112124. URL: <https://linkinghub.elsevier.com/retrieve/pii/S0034425720304971>, doi:[10.1016/j.rse.2020.112124](https://doi.org/10.1016/j.rse.2020.112124).
- 690        Taucare, M., Viguier, B., Figueiroa, R., Daniele, L., 2024. The alarming state of Central Chile's groundwater resources: A  
 691        22

- 700 paradigmatic case of a lasting overexploitation. *Science of The Total Environment* 906, 167723. URL: <https://linkinghub.elsevier.com/retrieve/pii/S0048969723063507>, doi:[10.1016/j.scitotenv.2023.167723](https://doi.org/10.1016/j.scitotenv.2023.167723).
- 701 Tennekes, M., 2018. tmap: Thematic Maps in R. *Journal of Statistical Software* 84, 1–39. doi:[10.18637/jss.v084.i06](https://doi.org/10.18637/jss.v084.i06).
- 702 Urrutia-Jalabert, R., González, M.E., González-Reyes, ., Lara, A., Garreaud, R., 2018. Climate variability and forest fires in central and south-central Chile. *Ecosphere* 9, e02171. URL: <https://esajournals.onlinelibrary.wiley.com/doi/10.1002/ecs2.2171>, doi:[10.1002/ecs2.2171](https://doi.org/10.1002/ecs2.2171).
- 703 Van Loon, A.F., Gleeson, T., Clark, J., Van Dijk, A.I., Stahl, K., Hannaford, J., Di Baldassarre, G., Teuling, A.J., Tallaksen, L.M., Uijlenhoet, R., Hannah, D.M., Sheffield, J., Svoboda, M., Verbeiren, B., Wagener, T., Rangecroft, S., Wanders, N., Van Lanen, H.A., 2016. Drought in the Anthropocene. *Nature Geoscience* 9, 89–91. doi:[10.1038/ngeo2646](https://doi.org/10.1038/ngeo2646).
- 704 Venegas-González, A., Juñent, F.R., Gutiérrez, A.G., Filho, M.T., 2018. Recent radial growth decline in response to increased drought conditions in the northernmost Nothofagus populations from South America. *Forest Ecology and Management* 409, 94–104. URL: <https://linkinghub.elsevier.com/retrieve/pii/S0378112717313993>, doi:[10.1016/j.foreco.2017.11.006](https://doi.org/10.1016/j.foreco.2017.11.006).
- 705 Venegas-González, A., Muñoz, A.A., Carpintero-Gibson, S., González-Reyes, A., Schneider, I., Gipolou-Zuñiga, T., Aguilera-Betti, I., Roig, F.A., 2023. Sclerophyllous Forest Tree Growth Under the Influence of a Historic Megadrought in the Mediterranean Ecoregion of Chile. *Ecosystems* 26, 344–361. URL: <https://link.springer.com/10.1007/s10021-022-00760-x>, doi:[10.1007/s10021-022-00760-x](https://doi.org/10.1007/s10021-022-00760-x).
- 706 Vicente-Serrano, S.M., Azorin-Molina, C., Sanchez-Lorenzo, A., Revuelto, J., López-Moreno, J.I., González-Hidalgo, J.C., Moran-Tejeda, E., Espejo, F., 2014. Reference evapotranspiration variability and trends in Spain, 1961–2011. *Global and Planetary Change* 121, 26–40. URL: <https://linkinghub.elsevier.com/retrieve/pii/S0921818114001180>, doi:[10.1016/j.gloplacha.2014.06.005](https://doi.org/10.1016/j.gloplacha.2014.06.005).
- 707 Vicente-Serrano, S.M., Beguería, S., López-Moreno, J.I., 2010. A multiscalar drought index sensitive to global warming: The standardized precipitation evapotranspiration index. *Journal of Climate* 23, 1696–1718. URL: <http://dx.doi.org/10.1175/2009JCLI2909.1>, doi:[10.1175/2009JCLI2909.1](https://doi.org/10.1175/2009JCLI2909.1).
- 708 Vicente-Serrano, S.M., Peña-Angulo, D., Beguería, S., Domínguez-Castro, F., Tomás-Burguera, M., Noguera, I., Gimeno-Sotelo, L., El Kenawy, A., 2022. Global drought trends and future projections. *Philosophical Transactions of the Royal Society A: Mathematical, Physical and Engineering Sciences* 380, 20210285. URL: <https://royalsocietypublishing.org/doi/10.1098/rsta.2021.0285>, doi:[10.1098/rsta.2021.0285](https://doi.org/10.1098/rsta.2021.0285).
- 709 Vicente-Serrano, S.M., McVicar, T.R., Miralles, D.G., Yang, Y., Tomas-Burguera, M., 2020. Unraveling the influence of atmospheric evaporative demand on drought and its response to climate change. *WIREs Climate Change* 11, e632. URL: <https://wires.onlinelibrary.wiley.com/doi/10.1002/wcc.632>, doi:[10.1002/wcc.632](https://doi.org/10.1002/wcc.632).
- 710 Wickham, H., Averick, M., Bryan, J., Chang, W., McGowan, L.D., François, R., Grolemund, G., Hayes, A., Henry, L., Hester, J., Kuhn, M., Pedersen, T.L., Miller, E., Bache, S.M., Müller, K., Ooms, J., Robinson, D., Seidel, D.P., Spinu, V., Takahashi, K., Vaughan, D., Wilke, C., Woo, K., Yutani, H., 2019. Welcome to the tidyverse. *Journal of Open Source Software* 4, 1686. doi:[10.21105/joss.01686](https://doi.org/10.21105/joss.01686).
- 711 Wilhite, D.A., Glantz, M.H., 1985. Understanding: The drought phenomenon: The role of definitions. *Water International* 10, 111–120. URL: <http://dx.doi.org/10.1080/02508068508686328>, doi:[10.1080/02508068508686328](https://doi.org/10.1080/02508068508686328).
- 712 Wilks, D.S., 2011. Empirical distributions and exploratory data analysis. *Statistical Methods in the Atmospheric Sciences* 100.
- 713 Winkler, K., Fuchs, R., Rounsevell, M., Herold, M., 2021. Global land use changes are four times greater than previously estimated. *Nature Communications* 12, 2501. URL: <https://www.nature.com/articles/s41467-021-22702-2>, doi:[10.1038/s41467-021-22702-2](https://doi.org/10.1038/s41467-021-22702-2).
- 714 WMO, Svoboda, M., Hayes, M., Wood, D.A., 2012. Standardized Precipitation Index User Guide. WMO, Geneva. URL: [http://library.wmo.int/opac/index.php?lvl=notice\\_display&id=13682](http://library.wmo.int/opac/index.php?lvl=notice_display&id=13682). series Title: WMO Publication Title: WMO-No. 1090 © Issue: 1090.
- 715 Wright, M.N., Ziegler, A., 2017. ranger: A Fast Implementation of Random Forests for High Dimensional Data in C++ and R. *Journal of Statistical Software* 77, 1–17. doi:[10.18637/jss.v077.i01](https://doi.org/10.18637/jss.v077.i01).
- 716 Wu, C., Zhong, L., Yeh, P.J.F., Gong, Z., Lv, W., Chen, B., Zhou, J., Li, J., Wang, S., 2024. An evaluation framework for quantifying vegetation loss and recovery in response to meteorological drought based on SPEI and NDVI. *Science of The Total Environment* 906, 167632. URL: <https://linkinghub.elsevier.com/retrieve/pii/S0048969723062599>, doi:[10.1016/j.scitotenv.2023.167632](https://doi.org/10.1016/j.scitotenv.2023.167632).
- 717 Xiao, C., Zaehle, S., Yang, H., Wigneron, J.P., Schmullius, C., Bastos, A., 2023. Land cover and management effects on ecosystem resistance to drought stress. *Earth System Dynamics* 14, 1211–1237. URL: <https://esd.copernicus.org/articles/14/1211/2023/>, doi:[10.5194/esd-14-1211-2023](https://doi.org/10.5194/esd-14-1211-2023).
- 718 Yang, J., Huang, X., 2021. The 30 m annual land cover dataset and its dynamics in China from 1990 to 2019. *Earth System Science Data* 13, 3907–3925. URL: <https://essd.copernicus.org/articles/13/3907/2021/>, doi:[10.5194/essd-13-3907-2021](https://doi.org/10.5194/essd-13-3907-2021).
- 719 Zambrano, F., 2023. Four decades of satellite data for agricultural drought monitoring throughout the growing season in Central Chile, in: Vijay P. Singh Deepak Jhajharia, R.M., Kumar, R. (Eds.), *Integrated Drought Management*, Two Volume Set. CRC Press, p. 28.
- 720 Zambrano, F., Lillo-Saavedra, M., Verbist, K., Lagos, O., 2016. Sixteen years of agricultural drought assessment of the biobío region in chile using a 250 m resolution vegetation condition index (VCI). *Remote Sensing* 8, 1–20. URL: <http://www.mdpi.com/2072-4292/8/6/530>, doi:[10.3390/rs8060530](https://doi.org/10.3390/rs8060530). publisher: Multidisciplinary Digital Publishing Institute.
- 721 Zambrano, F., Vrieling, A., Nelson, A., Meroni, M., Tadesse, T., 2018. Prediction of drought-induced reduction of agricultural productivity in Chile from MODIS, rainfall estimates, and climate oscillation indices. *Remote Sensing of Environment* 219, 15–30. URL: <https://www.sciencedirect.com/science/article/pii/S0034425718304541>, doi:[10.1016/j.rse.2018.10.006](https://doi.org/10.1016/j.rse.2018.10.006). publisher: Elsevier.
- 722 Zhang, W., Wei, F., Horion, S., Fensholt, R., Forkel, M., Brandt, M., 2022. Global quantification of the bidirectional de-

- 765 dependency between soil moisture and vegetation productivity. Agricultural and Forest Meteorology 313, 108735. URL:  
766 <https://linkinghub.elsevier.com/retrieve/pii/S0168192321004214>, doi:[10.1016/j.agrformet.2021.108735](https://doi.org/10.1016/j.agrformet.2021.108735).
- 767 Zhao, Y., Feng, D., Yu, L., Wang, X., Chen, Y., Bai, Y., Hernández, H.J., Galleguillos, M., Estades, C., Biging, G.S., Radke,  
768 J.D., Gong, P., 2016. Detailed dynamic land cover mapping of Chile: Accuracy improvement by integrating multi-temporal  
769 data. Remote Sensing of Environment 183, 170–185. URL: <https://linkinghub.elsevier.com/retrieve/pii/S0034425716302188>,  
770 doi:[10.1016/j.rse.2016.05.016](https://doi.org/10.1016/j.rse.2016.05.016).
- 771 Zhou, K., Li, J., Zhang, T., Kang, A., 2021. The use of combined soil moisture data to characterize agricultural drought  
772 conditions and the relationship among different drought types in China. Agricultural Water Management 243, 106479. URL:  
773 <https://linkinghub.elsevier.com/retrieve/pii/S0378377420305965>, doi:[10.1016/j.agwat.2020.106479](https://doi.org/10.1016/j.agwat.2020.106479).